Physics-based Risk Assessment of Compound Flooding from Tropical and Extratropical Cyclones in a Warming Climate

Ali Sarhadi[1], Raphael Rousseau-Rizzi[1], and Kerry A. Emanuel[1]

[1]Massachusetts Institute of Technology

February 15, 2024

Abstract

In recent years, efforts to assess the evolving risks of coastal compound surge and rainfall-driven flooding from tropical cyclones (TCs) and extratropical cyclones (ETCs) in a warming climate have intensified. While substantial progress has been made, the persistent challenge lies in obtaining actionable insights into the changing magnitude and spatially-varying flood risks in coastal areas. We employ a physics-based numerical hydrodynamic framework to simulate compound flooding from TCs and ETCs in both current and future warming climate conditions, focusing on the western side of Buzzard Bay in Massachusetts. Our approach leverages hydrodynamic models driven by extensive sets of synthetic TCs downscaled from CMIP6 climate models and dynamically downscaled ETC events using the WRF model forced by CMIP5 simulations. Through this methodology, we quantify the extent to which climate change can potentially reshape the risk landscape of compound flooding in the study area. Our findings reveal a significant increase in TC-induced compound flooding risk due to evolving climatology and sea level rise (SLR). Additionally, there is a heightened magnitude of compound flooding from ETCs, in coastal regions, due to SLR. Inland areas exhibit a decline in rainfall-driven flooding from high-frequency ETC events toward the end of the century compared to the current climate. Our methodology is transferable to other vulnerable coastal regions, serving as a valuable decision-making tool for adaptive measures in densely populated areas. It equips decision-makers and stakeholders with the means to effectively mitigate the destructive impacts of compound flooding arising from both current and future TCs and ETCs.

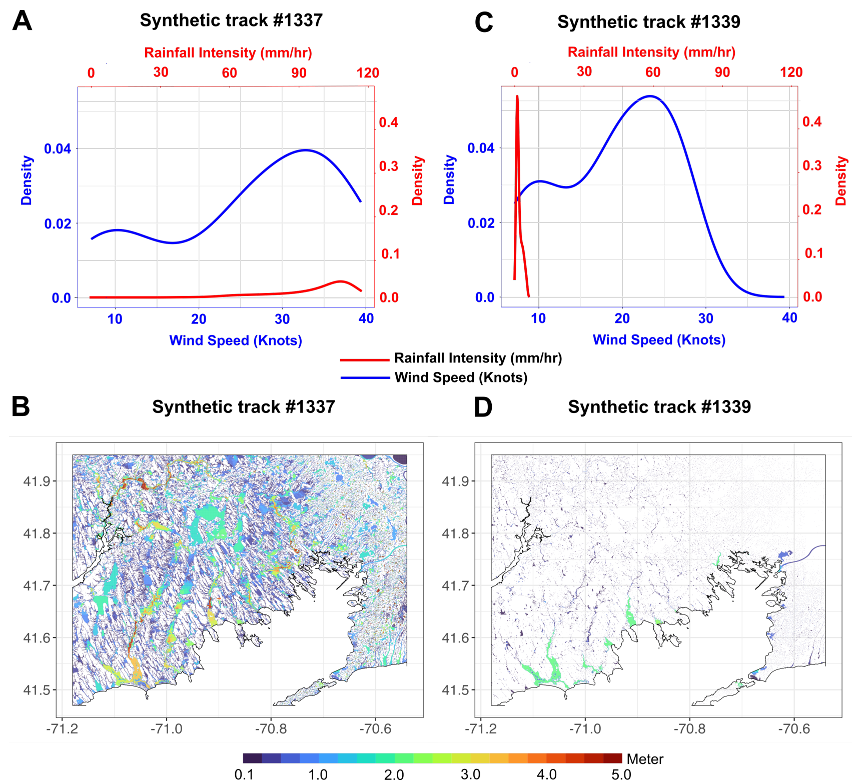

A
Synthetic track #1337
C
Synthetic track #1339
Rainfall Intensity (mm/hr)
Density
Wind Speed (Knots)
Rainfall Intensity (mm/hr)
Wind Speed (Knots)
B
Synthetic track #1337
D
Synthetic track #1339
Meter

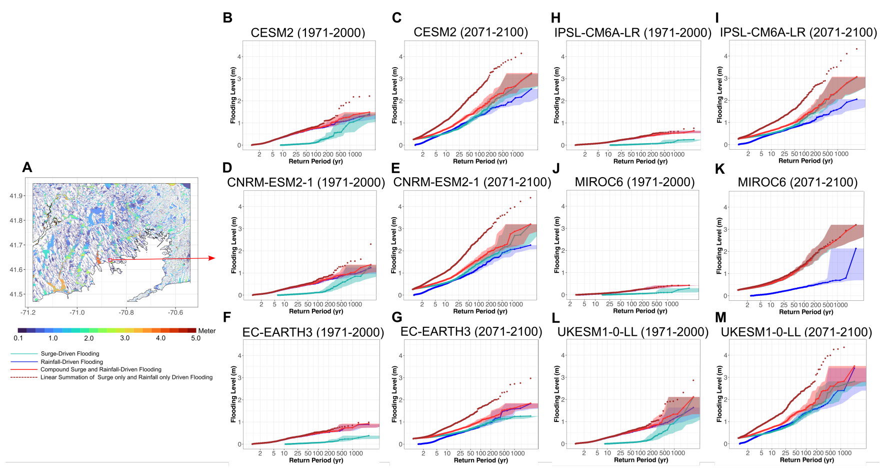

A
B
CESM2 (1971-2000)
C
CESM2 (2071-2100)
H
IPSL-CM6A-LR (1971-2000)
I
IPSL-CM6A-LR (2071-2100)
D
CNRM-ESM2-1 (1971-2000)
E
CNRM-ESM2-1 (2071-2100)
J
MIROC6 (1971-2000)
K
MIROC6 (2071-2100)
F
EC-EARTH3 (1971-2000)
G
EC-EARTH3 (2071-2100)
L
UKESM1-0-LL (1971-2000)
M
UKESM1-0-LL (2071-2100)

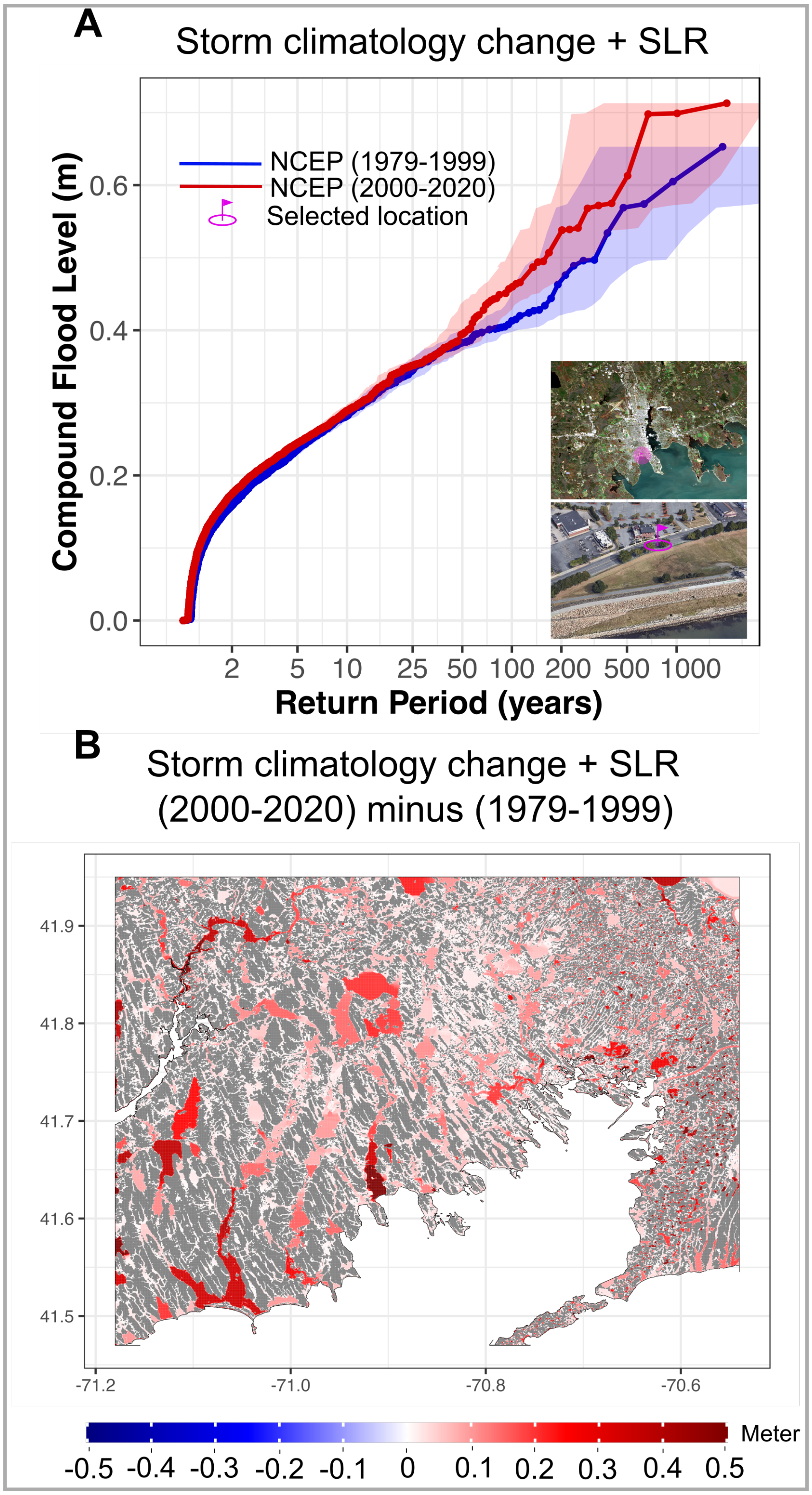
A
Storm climatology change + SLR
NCEP (1979-1999)
NCEP (2000-2020)
Selected location
Compound Flood Level (m)
0.0
0.2
0.4
0.6
2
5
10
25
50
100
200
500
1000
Return Period (years)
B
Storm climatology change + SLR
(2000-2020) minus (1979-1999)
41.9
41.8
41.7
41.6
41.5
-71.2
-71.0
-70.8
-70.6
Meter
-0.5 -0.4 -0.3 -0.2 -0.1 0 0.1 0.2 0.3 0.4 0.5

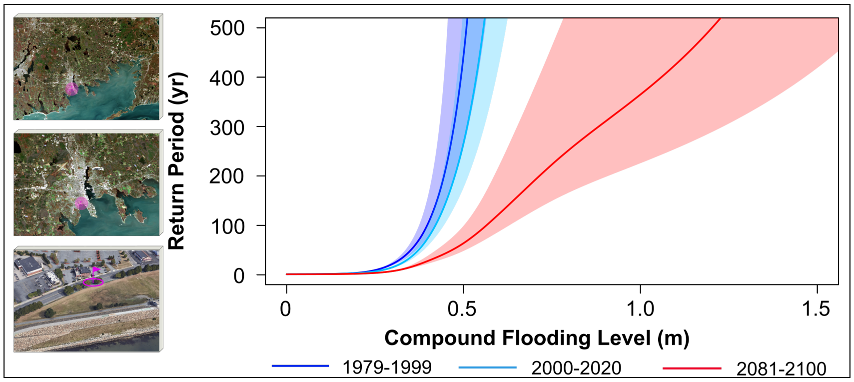

Return Period (yr)
500
400
300
200
100
0
0
0.5
1.0
1.5
Compound Flooding Level (m)
1979-1999
2000-2020
2081-2100

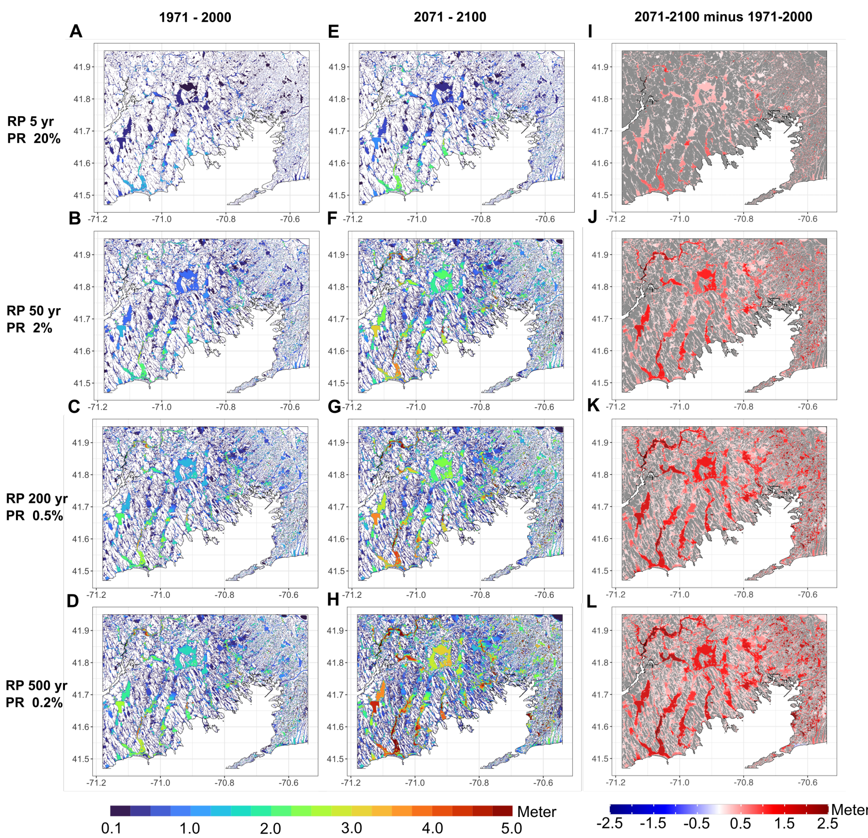

1971 - 2000
2071 - 2100
2071-2100 minus 1971-2000
A
B
C
D
E
F
G
H
I
J
K
L
RP 5 yr
PR 20%
RP 50 yr
PR 2%
RP 200 yr
PR 0.5%
RP 500 yr
PR 0.2%
Meter
0.1
1.0
2.0
3.0
4.0
5.0
Meter
-2.5
-1.5
-0.5
0.5
1.5
2.5

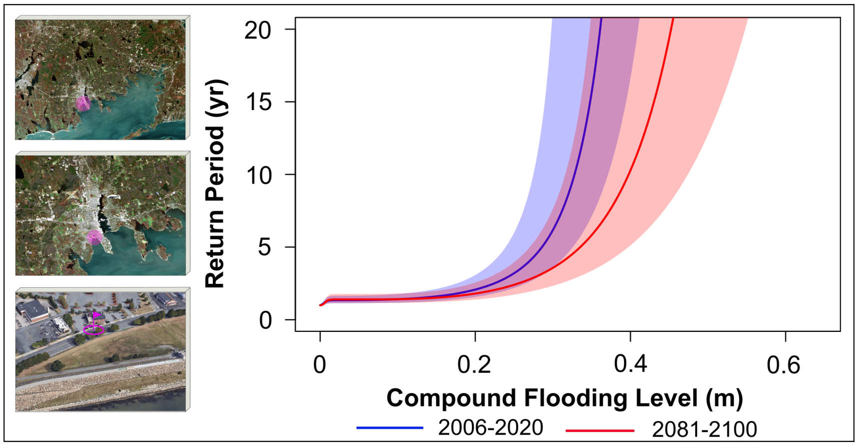
Return Period (yr)
Compound Flooding Level (m)
2006-2020
2081-2100

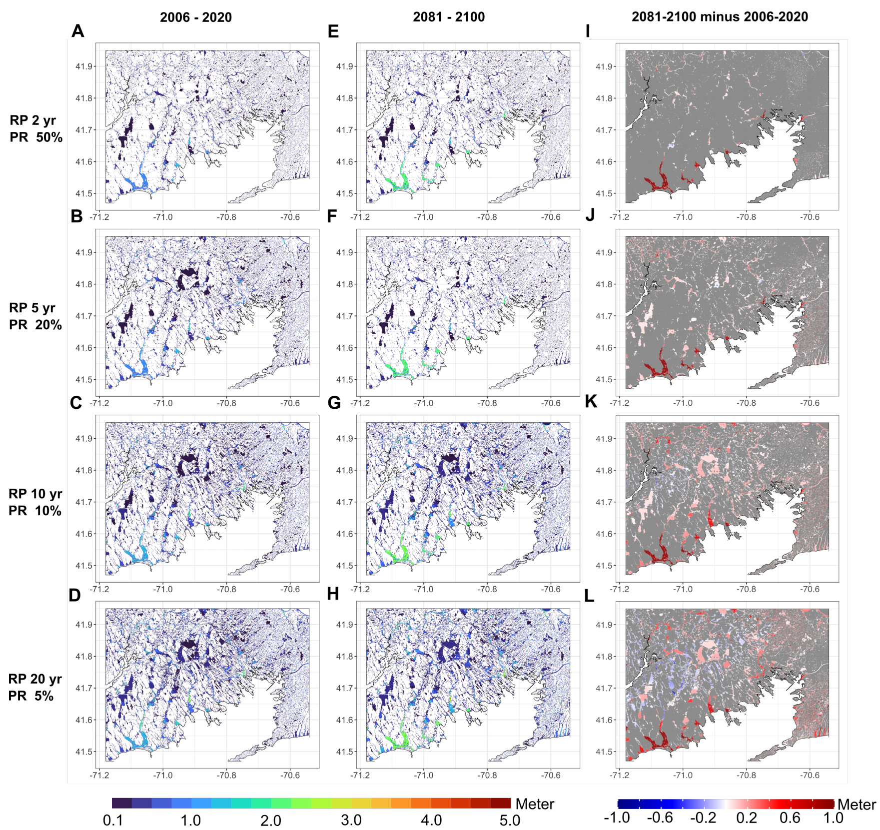
2006 - 2020
2081 - 2100
2081-2100 minus 2006-2020
RP 2 yr PR 50%
RP 5 yr PR 20%
RP 10 yr PR 10%
RP 20 yr PR 5%
Meter
Meter

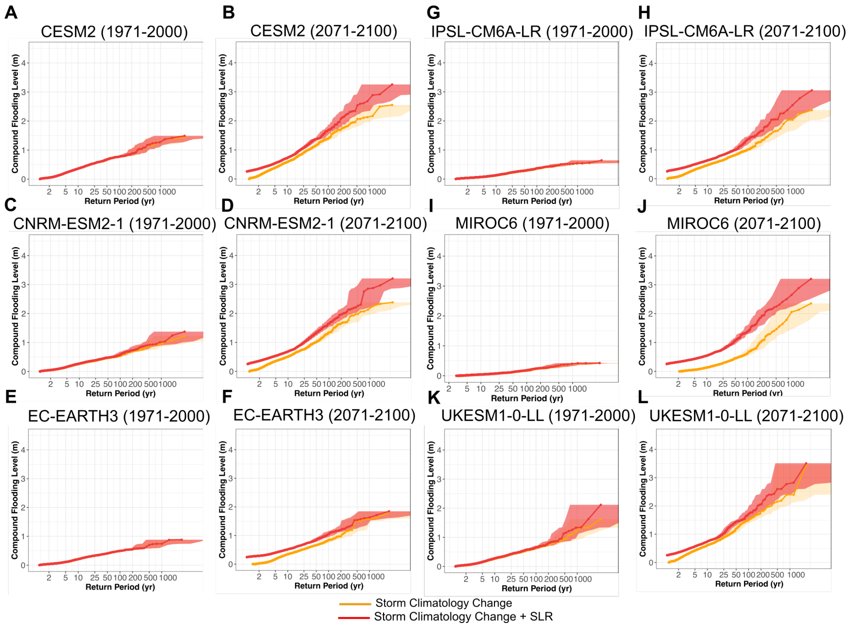
A
CESM2 (1971-2000)
B
CESM2 (2071-2100)
G
IPSL-CM6A-LR (1971-2000)
H
IPSL-CM6A-LR (2071-2100)
C
CNRM-ESM2-1 (1971-2000)
D
CNRM-ESM2-1 (2071-2100)
I
MIROC6 (1971-2000)
J
MIROC6 (2071-2100)
E
EC-EARTH3 (1971-2000)
F
EC-EARTH3 (2071-2100)
K
UKESM1-0-LL (1971-2000)
L
UKESM1-0-LL (2071-2100)
Compound Flooding Level (m)
Return Period (yr)
Storm Climatology Change
Storm Climatology Change + SLR

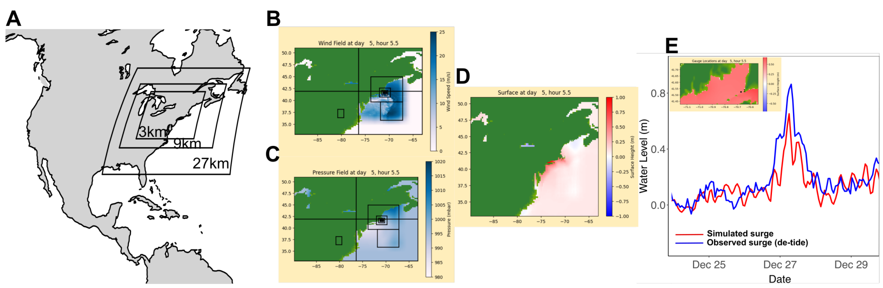
A
3km
9km
27km
B
Wind Field at day 5, hour 5.5
C
Pressure Field at day 5, hour 5.5
D
Surface at day 5, hour 5.5
E
Water Level (m)
Simulated surge
Observed surge (de-tide)
Dec 25
Dec 27
Dec 29
Date

Physics-based Risk Assessment of Compound Flooding from Tropical and Extratropical Cyclones in a Warming Climate

Ali Sarhadi[1], Raphaël Rousseau-Rizzi[1], and Kerry Emanuel[1]

[1]Lorenz Center, Department of Earth Atmospheric and Planetary Sciences, Massachusetts Institute of Technology, Cambridge, MA, USA

Key Points:

- Compound flooding
- Physics-based risk modeling
- Tropical and extratropical cyclones

Corresponding author: Ali Sarhadi, `sarhadi@mit.edu`

Abstract

In recent years, efforts to assess the evolving risks of coastal compound surge and rainfall-driven flooding from tropical cyclones (TCs) and extratropical cyclones (ETCs) in a warming climate have intensified. While substantial progress has been made, the persistent challenge lies in obtaining actionable insights into the changing magnitude and spatially-varying flood risks in coastal areas. We employ a physics-based numerical hydrodynamic framework to simulate compound flooding from TCs and ETCs in both current and future warming climate conditions, focusing on the western side of Buzzard Bay in Massachusetts. Our approach leverages hydrodynamic models driven by extensive sets of synthetic TCs downscaled from CMIP6 climate models and dynamically downscaled ETC events using the WRF model forced by CMIP5 simulations. Through this methodology, we quantify the extent to which climate change can potentially reshape the risk landscape of compound flooding in the study area. Our findings reveal a significant increase in TC-induced compound flooding risk due to evolving climatology and sea level rise (SLR). Additionally, there is a heightened magnitude of compound flooding from ETCs, in coastal regions, due to SLR. Inland areas exhibit a decline in rainfall-driven flooding from high-frequency ETC events toward the end of the century compared to the current climate. Our methodology is transferable to other vulnerable coastal regions, serving as a valuable decision-making tool for adaptive measures in densely populated areas. It equips decision-makers and stakeholders with the means to effectively mitigate the destructive impacts of compound flooding arising from both current and future TCs and ETCs.

Plain Language Summary

During storms in coastal areas, strong winds can cause surge-driven flooding, and simultaneously, intense rainfall may lead to inland heavy rainfall-driven flooding. Sometimes, these two flooding sources coincide, forming compound surge and rainfall-driven flooding, which is more destructive than either hazard alone. To assess the risk of such destructive compound flooding, we use physics-based models to quantify the frequency and magnitude of these hazards. Additionally, we evaluate how climate change and factors such as sea-level rise may affect the frequency and magnitude of such events in coastal areas. Through these detailed, granular risk assessments, regions facing increased flooding threats can develop strategies to better mitigate damages posed by compound flooding during extreme storms.

1 Introduction

Tropical cyclones (TCs) are powerful storms characterized by their strong winds, heavy precipitation, and storm surges. They predominantly affect tropical coastal areas, where they can cause significant annual damage, estimated at US$26 billion in the United States alone (Bakkensen & Mendelsohn, 2019). However, recent scientific evidence indicates a notable poleward shift in TC distribution. This shift is attributed in part to global climate warming and ocean temperature rise, which create conducive conditions for the formation and propagation of TCs into higher latitudes (Kossin et al., 2014; Kossin, 2018). As TCs extend into higher latitudes, they introduce new challenges and hazards. These areas are less accustomed to such extreme weather events, and their populations, infrastructure, and ecosystems may be poorly prepared to cope with them (Studholme et al., 2022). In addition to TCs occurring during warm seasons, extratropical cyclones (ETCs) develop in cold seasons in these regions. ETCs can experience slower movement as a result of atmospheric conditions, leading to intricate storm dynamics and an elevated likelihood of causing substantial damage (Booth et al., 2021; Colle et al., 2015).

Damage resulting from TCs and ETCs is associated with various hazards inherent to these weather systems. Strong winds and the low-pressure systems accompanying these storms during landfall can induce storm surges in coastal regions, leading to coastal flooding. Subsequently, during landfall, heavy rainfall can result in inland freshwater flooding. At times, both forms of flooding can transpire simultaneously, resulting in a compound event that combines salty storm surge and freshwater rainfall-driven flooding. The intricate interplay between these two sources of flooding often results in compound flooding events that exhibit greater destructive potential compared to individual occurrences of either saltwater surge or torrential freshwater rainfall-driven flooding (Wahl et al., 2015).

In a warming climate, several factors may contribute to an increased potential for compound flooding events resulting from TCs and ETCs. It is well-established that the intensity of rainfall associated with these storms is likely to intensify. This escalation is primarily driven by higher saturation vapor pressure of water, as dictated by the Clausius-Clapeyron equation (Liu et al., 2019). Furthermore, the movement of TCs toward higher latitudes, alterations in their translational speed, and modifications in the behavior of ETCs all contribute to the altered hazards associated with these storms (Kossin, 2018; Booth et al., 2021). Additionally, the rising sea levels further exacerbate the impact of compound flooding events, necessitating a comprehensive evaluation and mitigation of the associated risks (Strauss et al., 2021; Marsooli et al., 2019; Lin et al., 2019, 2016). It is important to gain a deeper understanding of how these alterations in storm characteristics, manifesting within a future warming climate, may reshape the risk of compound flooding resulting from these storms. This is particularly vital in regions unaccustomed to such cyclonic activity, as this knowledge is essential for enhancing preparedness, facilitating adaptation, and formulating mitigation strategies aimed at reducing the potentially devastating damages associated with these events.

One significant challenge associated with TCs and ETCs is the limited availability of comprehensive records of these storms. The most reliable records we can obtain date back only to the early satellite era, starting in the 1980s. This timeframe is relatively short, and for specific regions, some landfalling storms may not have been recorded, exacerbating the issue. Consequently, when attempting to employ historical records to quantify the risk of compound flooding from these storms, a significant degree of uncertainty arises due to the brevity of the dataset and the paucity of observations. Even if more extended records of these storms were available from the past, they may not be representative of today's climate, primarily due to the influence of climate change. It is important to emphasize that even contemporary climate records do not provide an accurate representation of future conditions, again owing to ongoing climate change. Therefore, any statistical risk assessment method relying solely on historical statistics may fail to accurately quantify the risk. Infrastructure or adaptation planning based on such methodologies can thus lead to vulnerabilities and significant damages. To address this data limitation and account for the evolving climate, we employ a physics-based risk modeling framework (Sarhadi et al., 2024). This framework is driven by the atmospheric and ocean climatology of reanalysis data and General Circulation Models (GCMs) (Emanuel et al., 2006, 2008; Komurcu et al., 2018). It enables the downscaling of TCs and ETCs across past, current, and future climate scenarios. This approach helps address the dearth of observations and provides insights into how these storms may evolve under a warming climate, consequently shedding light on how the risk of compound flooding in coastal areas at higher latitudes may change.

Compound flooding arises from the complex interplay between storm surge and heavy rainfall-driven inundation, manifesting across both spatial and temporal dimensions. It is important to meticulously model this intricate hydrodynamic interaction between the two sources of flooding, distinguished by their saline (surge) and freshwater (rainfall) characteristics, with a high level of temporal and spatial precision. In recent years, there has been a growing focus on modeling intricate coastal hydrodynamics. Commonly, statistical methodologies are used to assess flood risk by establishing joint statistical distributions that capture interdependencies among various flooding drivers, often at localized or gauge scales (Gori et al., 2020; Wahl et al., 2015; Moftakhari et al., 2017; Gori & Lin, 2022; Zhang & Najafi, 2020). However, these methods have limitations, primarily stemming from their inability to account for the complex dynamic interactions between storm surge and rainfall-driven flooding. These approaches rely heavily on statistical measures of dependence, which can introduce uncertainties. Moreover, they often overlook hydraulic dynamics of compound flooding, which involves integrating surge height and rainfall intensity to determine flooding levels while considering their compounded effects. The prevailing statistical practices, which often treat the drivers of compound flooding (rainfall intensity and surge height) through joint distributions rather than considering the actual hydraulically driven flooding, result in imprecise assessments of compound flooding risk. Numerous studies have explored coastal flooding stemming from TCs and ETCs through the utilization of physics-based modeling methodologies (Marsooli et al., 2019; Gori et al., 2020; Emanuel, 2017; Lin et al., 2019). However, the majority of these studies have primarily focused on single hazard scenarios, such as rainfall- or surge-induced flooding, or on combining separate hazards. Therefore, these approaches may underestimate flooding risk when modeling the hydrodynamics of compound flooding. In our study, we employ an innovative approach designed to overcome the limitations often associated with these conventional methodologies. Our method utilizes a physically-based numerical hydrodynamic model, allowing for the explicit simulation of compound flooding. This is accomplished by concurrently converting key driving factors, such as wind speed and rainfall intensity, into hydraulic-based flood simulations, providing a high level of temporal and spatial resolution to comprehensively capture the complex interplay between surge and rainfall-driven flooding during the landfall of TC or ETC storms.

By utilizing a state-of-the-art dataset of downscaled storms, combined with an understanding of the climatology of these storms and projected sea level rise (SLR) in the current and future warming climate, we can evaluate the potential evolution of compound flooding risk in coastal areas. This approach also allows us to identify the primary drivers that may intensify the risk of compound flooding. Such information can furnish a detailed granular perspective on the risk of compound flooding in coastal regions, enabling authorities to enhance their preparedness and adaptation strategies for coastal cities and communities. This proactive approach is crucial for mitigating damages in the current and future climates.

2 Dataset and methodology

Synthetic Tropical Cyclone Model and Datasets

To comprehensively address the multiple hazards associated with TCs, we initiate the process by creating synthetic TC events using the methodology detailed in references (Emanuel et al., 2006, 2008). This method employs deterministic and numerical downscaling to generate synthetic TCs by introducing random seeding, both in terms of their spatial and temporal characteristics, across the entire Atlantic Ocean basin. The initial wind intensity of these seeded TCs is determined through a deterministic calculation, utilizing a high-resolution, coupled ocean-atmosphere tropical cyclone model. This model is driven by the thermodynamic conditions of the ocean and atmosphere, taking into account various factors, including monthly mean sea surface temperature, atmospheric temperature, humidity, and daily interpolated horizontal winds at altitudes of 250 and 850 hPa (Emanuel et al., 2008).

It's important to note that any storms failing to intensify to wind speeds exceeding 21 m/s (equivalent to 40 knots) are excluded from the dataset. In a natural selection process, only seed vortices encountering favorable large-scale environmental conditions intensify into TCs, with their development timing synchronized with environmental climatic patterns. The intensity of TCs is determined through the employment of the Coupled Hurricane Intensity Prediction System (CHIPS), which is an axisymmetric hurricane model coupled to a 1D ocean model (Emanuel et al., 2004). For the purposes of this study, we fix the TC outer radius at 400 km, but otherwise, the structure of the vortex, including the radius of maximum winds, is determined by the model physics. The dynamic downscaling method enables the simulation of numerous synthetic TC events, driven by bias-corrected climate reanalysis or projections from CMIP6 GCMs. Throughout the entire lifespan of each synthetic TC, we consistently record key meteorological parameters, including maximum surface wind speed, pressure, and the radius of maximum winds. These parameters are obtained through the model and are saved at 2-hour intervals. Subsequently, a hydrodynamic model known as GeoClaw (Mandli & Dawson, 2014) is employed to simulate wind-induced storm surges with high temporal resolution along the coastline near the study area during the landfall of each synthetic TC (further details on this modeling process can be found in the provided references).

In addition to generating primary drivers for storm surges from synthetic TCs, we also generate high-resolution hourly rainfall intensity data at a spatial resolution of approximately 20 meters for the vicinity of the study area during the landfall of each synthetic TC using a Tropical Cyclone Rainfall (TCR) model (Feldmann et al., 2019). TCR, a physics-driven model, links convective rainfall in TCs to the TC vortex's vertical velocity, accounting for factors such as frictional convergence, topography, vortex stretching, baroclinic effects, and radiative cooling. Previous studies have applied TCR in risk assessments (Emanuel, 2017; Gori & Lin, 2022) and validated it against observed TC-related rainfall in the United States (Feldmann et al., 2019; Xi et al., 2020). These studies demonstrated TCR's accuracy in replicating coastal rainfall patterns but noted limitations in inland and mountainous areas. To assess the accuracy of this rainfall dataset, Feldmann et al., (2019) conducted an evaluation by comparing it with observed rainfall data obtained from the NEXRAD radar network and rain gauges across the eastern United States. This high-resolution, hourly rainfall intensity data plays a critical role in quantifying the rainfall-induced hazard, a key component contributing to the compound flooding processes.

The downscaling process is implemented for six distinct CMIP6 climate model simulations: CESM2, CNRM-ESM2-1, EC-EARTH3, IPSL-CM6A-LR, MIROC6, and UKESM1-0-LL, all operating under the SSP3-7.0 scenario. Synthetic TC tracks are generated for two different time periods: the late 20th century, spanning 1971-2000, and the end of the century, from 2071-2100, using the climate model simulations. The whole dataset comprises approximately 46,800 synthetic storms, with approximately 3,900 synthetic storms generated from each climate model in each period. Furthermore, we repeat this process to generate 4,100 synthetic storms based on NCEP reanalysis data, representing the late 20th century and current climates (1979-2020). In total, these datasets encompass a large set of synthetic TCs, with their centers passing within 300 km of the New Bedford city in the study area.

Extratropical cyclone datasets

The method described above, which involves statistically and deterministically downscaling TCs, enables the simulation of a vast number of idealized synthetic TC events based on climate reanalysis or climate model simulations (Emanuel et al., 2008). This is possible, to a reasonable extent, because the feedback of TCs on the surrounding large-scale environment does not significantly impact their subsequent evolution. For example, TC tracks are primarily determined by the large-scale flow in which they are embedded (and, to a lesser extent, by the beta drift effect), which passively advects them (Emanuel et al., 2006), irrespective of the TC's internal evolution. Additionally, this method employs analytical simplifications, such as assuming axisymmetry and moist slantwise-neutrality in the free troposphere, which reduces the downscaling model to a single radial dimension, making it computationally efficient, even at high radial resolution.

However, for ETC events, it is not feasible to neglect the effects of the storm on the large-scale environment. Therefore, it is not possible to generate additional synthetic ETCs within a given global climate model run. Only storms explicitly simulated in these runs can be dynamically downscaled. At present, there are no reduced-dimension models that can be used to dynamically downscale ETCs, so computationally expensive regional climate models like the Weather Research and Forecasting (WRF) model (Komurcu et al., 2018) are required to provide high-resolution information on the behavior of ETCs for risk assessment. Due to the difficulty and computational cost associated with simulating a large number of downscaled ETC events, we do not attempt to do this ourselves. Instead, we utilize state-of-the-art WRF dynamical downscaling data described in Komurcu et al., (2018). These downscaling simulations were developed to support regional climate studies in the northeastern U.S. They downscale CMIP5, RCP8.5 projections by CESM v1.0, which have been bias-corrected to support climate research. The WRF data used here covers two different time periods: the 2006-2020 current climate period and the 2081-2100 end-of-the-century period, with hourly time resolution. Additionally, we use the output of a 2006-2015 WRF simulation to downscale ERA-Interim reanalysis data (Dee et al., 2011), which aids in verifying our model. The WRF simulations employ nested domains on a Cartesian grid, with the innermost domain covering 1500 km by 1200 km and using uniform convection-permitting 3 km resolution. To simulate rainwater flooding and storm surge in the study area, we require downscaled precipitation rates, surface pressure, and surface winds, which must be transformed from the WRF Lambert conformal conic projection to the geographical coordinates used in the hydraulic and surge models. More detailed information can be found in Sarhadi et al. (2024).

To assess the risk associated with compound flooding, we compile a catalog of potential freshwater and surge flooding events linked to ETCs for each downscaled period. To identify potential freshwater flooding events, we calculate time series of rainfall intensity averaged over the area extending from -71.2 to -70.5 W and 41.5 to 41.9 N for each historical and future period. Potential freshwater flooding events are selected iteratively by searching for rainfall intensity maxima in the time series in decreasing order, starting from the global maximum. Each event extends from four days before to one day after the selected local maximum. Once an event is defined, its full time-span is removed from the time series so that the next, slightly weaker event selected is the most intense remaining event in the time series. The total number of events selected in each downscaled period is equal to five times the number of years in the corresponding period. Similarly, to identify potential surge flooding events, we select maxima in a time series of the wind component oriented toward the coast averaged over a 2° × 2° box off the coast of the western Buzzards Bay area. It's important to note that the instantaneous precipitation intensity averaged over the study area and the average wind component oriented toward the coast are only rough predictors of freshwater and storm surge flooding. However, the number of selected rainfall and wind events is sufficient to ensure that all events capable of producing significant freshwater or surge flooding are included. To avoid including tropical cyclones, we only seek events occurring between October and May. We acknowledge that there may be some overlap between TCs and ETCs in October.

Storm surge modeling

Consistent with previous research (Reed et al., 2015; Lin et al., 2016; Garner et al., 2017), we define a storm surge as the anomalous elevation of sea level above Relative Sea Level (RSL). This elevation results from the low atmospheric surface pressure and the high surface wind speed associated with TCs or ETCs. The combination of storm surge and RSL fluctuations characterizes the surge height in coastal regions caused by TCs and ETCs. Our RSL estimation is based on the local average of the total sea level throughout each climate period. RSL also serves as the key factor for distinguishing between land and water elevations. As a result, we disregard interannual sea level variations and the relatively minor nonlinear interactions between the surge and RSL, as outlined in prior studies (Lin et al., 2016). Furthermore, astronomical tides are not factored into our calculations. It is important to note that future studies should investigate the effects of tides and their nonlinear interactions with surges, particularly in light of potential changes due to SLR (Müller, 2011; Garner et al., 2017).

To simulate storm surges generated by synthetic TCs and ETCs, we utilize the GeoClaw numerical model, which relies on high-resolution shock-capturing finite volume methods (Mandli & Dawson, 2014). Unlike finite-element unstructured hydrodynamic models (Colle et al., 2008; Westerink et al., 2008), GeoClaw incorporates Adaptive Mesh Refinement (AMR) algorithms (Berger et al., 2011; Mandli & Dawson, 2014), enabling efficient computational solutions at high resolutions over large scales. We implement a broad domain, covering approximately 1000 kilometers, to better quantify the large-scale impact of various attributes of TCs and ETCs, including intensity, duration, size, and landfall location, on storm surges. Along the coastline in the study area, we position synthetic gauges to provide comprehensive coverage. These gauges record surge heights at high temporal resolutions, typically less than a minute, during each individual landfall of TCs and ETCs. We also employ an interpolation method to derive surge heights at additional synthetic gauges distributed along the entire coastline. Consequently, these coastal surge conditions are transformed into surge-driven flooding through a hydraulic model, allowing us to model the propagation of surges and their potential to cause surge-driven flooding in coastal areas. This surge simulation approach is applied to a broad set of synthetic TC and ETC events. It's worth noting that the performance of GeoClaw in modeling TC surges has been evaluated in previous studies (Miura et al., 2021; Mandli & Dawson, 2014; Sarhadi et al., 2024). Through the incorporation of critical enhancements, we have expanded GeoClaw's functionality to effectively model storm surges resulting from ETCs, thereby surpassing the default settings of the out-of-the-box model.

Figure 1 illustrates the surge modeling process, which entails dynamically downscaled WRF simulations of primary surge drivers, including wind and pressure fields, forced by ERA-Interim reanalysis data. The simulation corresponds to a historical ETC event that occurred on December 27-28, 2012, within the study area. The model's performance accuracy is depicted in Figure 1. The simulated surge, using the modified GeoClaw model, demonstrates a robust agreement with observed surge levels. These observed surge values were obtained by de-tiding water levels, a procedure that involves subtracting water elevation from NOAA tide predictions at the Woods Hole gauge.

For modeling surges generated by TCs and ETCs during the late 20th century and in the current climate, we rely on RSL data obtained from NOAA gauge observations. However, in the context of future climate scenarios, we incorporate SLR projections derived from CMIP6 under the SSP3-7.0 scenario into GeoClaw using a bathtub approach. This allows us to quantify the impact of SLR on the changing risk of surges and compound flooding. The methodology involves calculating the ensemble mean of total SLR over future climate scenarios (Fox-Kemper et al., 2021). These projections encompass comprehensive considerations, including the contributions of Antarctic and Greenland ice sheets, glacier dynamics, thermal expansion of seawater, terrestrial water storage, vertical land motion, and the potential influences of marine ice cliff instability.

Numerical compound flood modeling

To simulate the intricate hydrodynamic interactions involved in compound flooding, a confluence of storm surges and heavy inland rainfall stemming from synthetic TCs and ETC events, we modified a version of the LISFLOOD-FP model. This two-dimensional hydraulic model, renowned for its high spatio-temporal resolution, is recognized for its computational efficiency. A detailed description of this model is provided in reference (Neal et al., 2012). LISFLOOD-FP employs an explicit finite difference scheme to simulate shallow water waves, while deliberately omitting advection (Bates et al., 2010). The efficacy of the fundamental model's numerical scheme in simulating pluvial and fluvial flood dynamics has been substantiated by various studies (Neal et al., 2012; Wing et al., 2022; Bates et al., 2021). In our work, this model has been customized to incorporate high-resolution surge height data (simulated by GeoClaw) along the coastline, and simultaneously, it accommodates hourly rainfall intensity data from storm events in the inland regions as boundary conditions. This physically based approach empowers the model to replicate the dynamics of compound flooding in response to the rapid spatio-temporal fluctuations in surge and rainfall driven flooding during the landfall of each storm. The model ensures the conservation of mass within each grid cell and maintains the continuity of momentum of compound flooding between neighboring cells. The model recalculates the flow depth, taking into account the elevation of each cell, water surface slope, surface Manning's roughness coefficient, and acceleration due to gravity. More details about the methodology can be found in Sarhadi et al. (2024).

It's important to note that the geodetic datum of NAD83 is utilized to establish the spatial coordinates, while the vertical datum of NAVD88 is used for elevation values within the applied Digital Elevation Model (DEM). In our study, we utilize a LiDAR-based DEM with an approximate spatial resolution of 20 m, employing a geographic (Lat/Lon) projection to represent the area's geometry. A land-use map is employed to quantify surface roughness, and a map of available soil water storage for the topsoil layer (0-50 cm) is used to account for the infiltration rate in non-constructed areas. The source of these input files is given in the data availability section.

In this process, the hydrodynamics of compound flooding during the landfall of each storm are comprehensively simulated with high temporal and spatial resolution. We then store the maximum compound flooding level at each grid cell for every individual storm event. This process is iteratively conducted for a vast set of TCs and ETCs derived from reanalysis and climate models. These maximum flood records serve as a reflection of the compound flooding behavior over each defined time period for every grid cell. Subsequently, these records are fundamental in constructing a nonparametric empirical Cumulative Distribution Function (eCDF). This approach leverages the theory of nonexceedance probability to determine the return period of a compound flooding event at each grid cell.

The calculation is expressed as:

$$T_H(h) = \frac{1}{P(H > h)} \tag{1}$$

In this equation, $P(H > h)$ signifies the annual probability that the compound flooding level of an event (H) exceeds a specific threshold (h), and $T_H(h)$ corresponds to the return period of that particular event. The ensemble mean of compound flooding levels for TCs and ETCs at various return periods is then computed by considering multiple climate models across distinct time periods. The assessment of expected changes in compound flooding levels at specific return periods is carried out by evaluating the disparities between the ensemble mean of flood levels in future climate scenarios and those in past or current climate conditions. To dissect the individual and collective influences of changes in storm climatology and SLR on the granular risk of compound flooding, our approach involves running the hydraulic model twice for each individual storm. This includes one simulation with the incorporation of SLR and another without it. This approach allows us to discern and quantify the distinct and synergistic effects of variations in storm climatology and SLR on the risk of compound flooding. To distinguish the contribution of each individual hazard (surge or rainfall-driven flooding) in compound flooding from each storm, we can simply run the model with only one driver as the boundary condition.

3 Results and Discussion

Impact of primary driver severity on compound flooding

Here, we evaluate the influence of the primary drivers during the landfall of TCs on the magnitude and extent of inundation associated with compound flooding in the study area. This assessment is pivotal for gaining a comprehensive understanding of the intricacies inherent in flood hazards stemming from these meteorological phenomena. High wind speeds and low atmospheric pressure during the landfall of TCs lead to storm surge-driven flooding along coastal regions. Specifically, the greater the wind speed, the more intense and higher the storm surge becomes both before and during landfall. Concurrently, rainfall intensity during landfall contributes to rainfall-driven flooding. The interplay between these factors, as elucidated in this study, sheds light on the intricate mechanisms that underpin the devastating consequences of compound flooding induced by TCs. The severity and dominance of each primary driver determine the corresponding severity of the compound flooding hazard. Depending on which primary driver predominates, it may result in scenarios such as compound flooding with a dominant surge in coastal areas, a situation where rainfall-driven flooding in inland areas is more pronounced, or instances when both drivers are strong, leading to a severe compound flooding event characterized by both surge and rainfall-driven inundation.

By examining the magnitude of these primary drivers, our study offers essential insights into the dynamics of compound flooding, encompassing factors like magnitude and the extent of inundation. To illustrate this, we selected two TCs as case studies to demonstrate how the magnitude of primary drivers can affect the resulting compound flooding. Figure 2 (top panels) presents information on the primary drivers of these two synthetic TC storms, which were derived from downscaling NCEP reanalysis data for the current climate. These measurements are presented both prior to landfall and at the time of landfall.

In the first case, represented by synthetic track #1337 (Fig. 2, A and B), the primary drivers include strong wind speeds (knots) at the eye of the TC before and during landfall, with rainfall intensity reaching up to 90-120 mm/hr in certain grid cells and an average wind speed of 40 knots (though it's important to consider the duration of high wind speeds too). These primary drivers result in flooding depths of up to 3 meters in some low-land coastal and inland areas. In contrast, the second case, depicted by synthetic track #1339 (Fig. 2, C and D), exhibits lower rainfall intensity, with the upper tail reaching up to 10 mm/hr, and wind speeds at the eye barely reaching 40 knots in the upper tail. These conditions lead to significantly lower flooding, especially in inland areas, and a reduced presence of compound flooding in coastal areas, where the flooding is predominantly surge-driven.

This understanding offers a comprehensive and scientifically robust exploration of the relationship between the magnitude of primary drivers—specifically, rainfall intensity and surface wind speed—and the resulting complex dynamics of compound flooding. These insights are invaluable for advancing our understanding of the multifaceted flood hazards associated with TCs, which, in turn, contribute to a more informed and resilient approach to disaster preparedness. Using this approach, one can easily quantify the proportion of each individual hazard and analyze the dynamic interplay between them in generating compound flooding, with high temporal and spatial resolution. Notably, the same methodology can be readily applied to ETC storms. This deeper understanding supports improved forecasting, risk assessment, and preparedness measures in vulnerable coastal regions, ultimately enhancing resilience against the impacts of these storms. In the subsequent section, we delve into the contribution of each individual and compound hazard to the risk assessment and emphasize the significance of a physics-based approach to compound flooding.

Assessing compound flooding impact and risk

In this section, we present a comparative analysis of compound flooding, delineating the individual contributions of surge and rainfall-driven flooding with a focus on coastal areas. The objective is to offer a clearer understanding of the effects and potential risks associated with compound flooding. Additionally, we examine how other approaches, such as singular hazards, surge, and rainfall-driven flooding considered individually, or a linearly additive hazards approach, may lead to the underestimation or overestimation of the risk. It is important to note that our comparisons are based on the results obtained from six climate models. This approach enhances clarity by visualizing differences in various sources of flooding within the models and accounting for uncertainties among them.

To better comprehend the impact and importance of compound flooding in risk assessment for both the late 20th and 21st century climates, we selected a specific coastal area, which is also an urban area, as depicted in Figure 3 (A). This area was chosen to predominantly consist of non-tidal ground areas, with intertidal zones excluded, facilitating a comparative risk analysis. We evaluated the risk, defined by probability of occurrence or return period, associated with single hazards: surge-driven flooding (represented in green), rainfall-driven flooding (in blue), and compound flooding, which takes into account the complex hydrodynamic interplay between these hazards at high temporal and spatial resolutions (depicted in red). We also included a linear addition of individual flooding as a commonly used approach (in brown). This comparative analysis is instrumental in discerning the biases that arise when individual hazards are considered separately or when the two are merely linearly combined to assess flooding risk, without accounting for the intricate hydrodynamic interactions across time and space inherent in compound flooding.

As depicted in Figure 3, during the late 20th century, a significant proportion of compound flooding contributions originated from rainfall-driven flooding rather than surge-driven flooding, for both high-frequency and low-frequency events in nearly all climate models. This emphasizes the risk underestimation resulting from relying solely on surge-driven flooding in this region. Conversely, the linear summation of the two individual hazards, without accounting for the complex hydrodynamics of their interaction during landfall, results in an overestimation of risk in the majority of the climate models.

Moving forward to assess the risk at the end of the 21st century, a significant increase is observed in both individual and compound flooding risks, driven by alterations in storm climatology and SLR. Although, compared to the 20th century, the risks of both rainfall-driven flooding and surge-driven flooding increase significantly; however, unlike the end of the 20th century, surge-driven flooding dominates and contributes more to compound flooding compared to rainfall-driven flooding in this area, especially for low-frequency events (with return periods above 50 years). For specific upper tail low-frequency events, there is a heightened prominence of surge-driven flooding, contributing to compound flooding (in almost all climate models except UKESM1-0-LL), compared to rainfall-driven flooding. Additionally, the risk of compound flooding intensifies; events that previously occurred once every 100 years in the late 20th century will pose a risk of occurring almost every less than 5 years by the end of the 21st century in almost all climate models. It is also worth noting that simply linearly summing the two single hazards together to assess compound flooding results in a significant overestimation of the risk in the future climate. For example, events that occur approximately every 500 years (factoring in the complex hydrodynamic interplay between surge and rainfall-driven flooding) are estimated to happen approximately every 75 years by the end of the century when individual hazards are simply added linearly, signifying a considerable bias and overestimation in risk assessment.

The results initially emphasize the significance of employing a physics-based model for downscaling TCs under the context of a future warming climate. This approach is crucial for an accurate assessment of risk, as it takes into account the influence of climate change in the forthcoming decades. This stands in contrast to relying solely on historical records, which do not accurately represent the characteristics of storms in the future warming climate and overlook the profound impacts of climate change on TC behavior. The results also underscore the importance of considering the explicit complex hydrodynamics interplay between the individual flooding hazards when assessing the risk, as neglecting it was the case in previous studies (Reed et al., 2015; Lin et al., 2016; Garner et al., 2017; Emanuel, 2017; Marsooli et al., 2019; Lin et al., 2012), can lead to a severe underestimation of the actual risk in both current and future climates, with the discrepancy becoming more pronounced due to changes in climatology and SLR.

Sea level rise and tropical cyclone climatology impacts

SLR and changes in TC climatology are recognized as the primary drivers behind alterations in the risk of compound flooding in coastal regions. SLR, largely attributed to global climate change, raises the baseline water level, rendering coastal areas more susceptible to inundation. When coupled with anticipated shifts in storm climatology, including variations in cyclone tracks, intensification, frequency, and other relevant attributes, the potential for compound flooding becomes increasingly evident. In this section, we investigate the compounding effects of SLR and changes in storm climatology, analyzing their influence on the risk of compound flooding during the late 20th century and the late 21st century. The late 20th century serves as a baseline for comprehending historical trends, while the late 21st-century projection offers insights into future warming scenarios.

Figure 4 shows the compound flooding level from a large set of synthetic tracks in the previously selected coastal area (depicted in Figure 3 (A)), both with and without SLR in the late 20th and 21st centuries, based on the output from six climate models. This analysis aims to better understand the effect of SLR on changing the risk of compound flooding and associated uncertainty within and among different climate models. In the late 20th century, as depicted in Figure 4, SLR does not exhibit a discernible effect on the risk of compound flooding caused by TCs. During this baseline period, the risk of experiencing compound flooding with a 0.5-meter depth, for example, is approximately 1% per annum on average, based on the ensemble of the six climate models, both with and without SLR. As we progress towards the end of the century, changes in storm climatology, without considering the SLR effect, are projected to elevate the risk of compound flooding events. This elevation is manifested with a 10% probability per annum based on the CNRM-ESM2-1 model (Figure 4-D). This projection indicates that changes in storm climatology alone will escalate the risk of 0.5-meter events tenfold compared to the late 20th century. However, when we consider the added contribution of SLR by the end of the century, the risk of a compound flooding event of this nature will increase significantly. It is projected to occur approximately with a 20% probability per annum. This signifies that the combined impact of SLR and changes in storm climatology will amplify the risk twentyfold compared to the late 20th century. Furthermore, SLR alone will elevate the occurrence of such compound flooding events tenfold compared to the late 20th century and increase the annual probability of such an event to 10%. Similar intensification patterns are observed in other climate models. The intensification resulting from the combined impact of SLR and changes in storm climatology significantly amplifies the risk of low-frequency events in the late 21st century. For instance, events that historically had a return period of 1000 years in the late 20th century are projected to occur 40 times more frequently by the end of the century in the majority of the models. In terms of the depth of compound flooding events with a return period of 1000 years in the selected coastal area, the EC-EARTH3 model estimates it to be approximately 0.75 meters (ranging from 0.6 to 0.8 meters) in the late 20th century. However, by the end of the century, the depth of events with the same return period is projected to be around 1.65 meters (ranging from 1.5 to 1.8 meters) due to the combined effects of SLR and changes in storm climatology.

Another noteworthy observation is that SLR is expected to significantly increase the risk of low-frequency events in the upper tail compared to other medium or high-frequency events by the end of the century. In a warming climate, all climate models (except EC-EARTH3 and UKESM1-0-LL) show that SLR is projected to intensify the risk significantly for upper tail events. For example, an extreme event that might occur almost once every 2000 years (based on the CNRM-ESM2-1 model) by the end of the century would have a depth of compound flooding without the impact of SLR at almost 2.4 meters. However, with SLR's impact by that time, the depth is projected to increase to around 3.3 meters in such a warming climate. This difference is smaller in medium to high-frequency events.

Our methodology enables us to examine and elucidate how these interacting primary drivers may influence the risk of compound flooding in a warming climate, providing valuable insights into the adaptive strategies and mitigation measures required for the late 21st century to safeguard coastal communities and infrastructure in an evolving climate. These analyses furnish detailed granular information about which primary drivers are of greater concern and how adaptive strategies can be tailored for each specific area based on priorities.

Tropical cyclone compound flooding risk in today's climate

Here, we utilize our methodology to quantitatively assess the impact of anthropogenic warming that has already occured on the risk of compound flooding, specifically through TC climatology and SLR, within the context of the current climate in the study area. To achieve this, we conduct simulations to determine the maximum compound flooding levels from 4,100 synthetic TCs. These TCs are downscaled from NCEP reanalysis data for two distinct climate periods: the late 20th century (1979-1999) and the early 21st century (2000-2020). Figure 5 (A) illustrates alterations in the level of compound flooding events for different return periods between these two time frames, focusing on a selected location close to the shore, encompassed by buildings and road networks.

Our results suggest no significant changes in the risk of high-frequency events (less than 50 years) in the current climate compared to the late 20th century. Furthermore, they suggest a slight increase in the magnitude of compound flooding, characterized by return periods exceeding 50 years, under today's climate compared to the late 20th century. This intensification is observed for rare events as well. However, it is important to note that distinguishing distinct trends for these events proves challenging due to sampling uncertainties.

In Figure 5 (B), we present the spatially distributed risk of compound flooding events occurring once every 100 years or with a 1% likelihood of occurring in any given year across the entire study area. The outcomes suggest that climate change has notably elevated the flood levels associated with such events, particularly in low-land coastal and inland areas, resulting in an increase of up to 0.4 meters, though the sampling uncertainty is large at these return periods. Notably, there is no observed decrease in the level of flooding within the region. These results underscore the profound influence of climate change on TC characteristics, including wind speeds, in conjunction with SLR, intensified rainfall, and the consequential surge height and compound flooding along coastlines, as well as inland flooding. Our findings underscore the pivotal role of climate change in reshaping the risk of compound flooding in the study area. A nuanced understanding of this evolving risk provides valuable insights for decision-makers, even in the short term, within the current climate as compared to the past. This knowledge aids in identifying areas that are most vulnerable to these hazards, thereby facilitating more informed decision-making processes in the current climate.

Tropical cyclone compound flooding risk in a future warming climate

Here, we conduct a comprehensive analysis of compound flooding risk associated with TCs, focusing on how this risk may evolve in a warming climate. Our investigation considers changes in TC climatology and SLR across different time periods. To understand the temporal evolution of compound flooding risk in our study area, we center our analysis on a specific location near New Bedford City, as indicated in Figure 6. Our aim is to illuminate the changing dynamics of compound flooding depths in this area, drawing insights from historical data, contemporary observations, and future climate projections.

We conducted a rigorous probabilistic analysis, employing advanced mixture modeling techniques to delineate the underlying probability distributions of compound flooding for each time period. Specifically, gamma and Weibull mixture models were applied to simulated compound flooding levels from each climate model, with model selection guided by the Akaike Information Criterion (AIC). To comprehensively assess inherent uncertainty, we applied bootstrap resampling techniques, generating 3,000 samples per iteration for compound flooding level simulations from each climate model across each time period. Subsequently, confidence intervals at the 5% and 95% levels were derived for key parameters associated with the fitted distribution. The frequency of compound flooding in the specified regions, attributed to changes in storm climatology and SLR, is delineated in Figure 6 through aggregated simulations involving six CMIP6 climate models. In this figure, the bold line represents the frequency of compound flooding levels within the selected area for different return periods across distinct time periods, including simulations for the late 20th and 21st centuries, as well as reanalysis data from the NCEP dataset for the current climate. Furthermore, the colored envelope illustrates the ensemble mean within the 5th to 95th percentile range, calculated based on the outcomes derived from the six climate models. The results (based on the ensemble mean of the climate models) indicate that compound flooding events that previously occurred with a 1% probability in a given year, in the late 20th century in this particular location, have now increased in frequency. In the current climate, these events occur with an annual probability of 1.3 in any given year, and in the future, they are expected to occur with a probability of 3.3 in each year. Evidently, changes in storm climatology and SLR are leading to a significant increase in the risk of compound flooding in the selected area. Furthermore, in a future warming climate, the depth of compound flooding associated with low-frequency events from TCs will also substantially increase. For instance, for events with an annual probability of 0.2%, the depth of compound flooding in this specific area is projected to rise from approximately 0.5 meters in the current climate to 1.25 meters by the end of 21st century. Therefore, it is crucial that the design of infrastructure, housing, and other critical facilities takes into account the heightened risk of compound flooding from TCs, both in the present and in the face of future, intensifying storms and SLR.

To gain a comprehensive understanding of the spatially distributed risk of compound flooding in the area, we have calculated the risk for each grid cell with a 20-meter spatial resolution, drawing from the extensive simulations of synthetic TCs. Figure 7 illustrates the results for different types of compound flooding events with return periods of 5, 50, 200, and 500 years. This spatial analysis provides valuable insights into the risk associated with both high-frequency and low-frequency compound flooding events from TCs. For each time period, including the late 20th century (Figure 7 A-D) and the 21st century (Figure 7 E-H), we assessed the depth of compound flooding for various high and low-frequency events at the grid cell level. To understand the role of changes in storm climatology and SLR in reshaping the risk landscape of compound flooding in warming climate in the study area, we have used the late 20th century as a baseline for comparison. The ensemble mean of compound flooding for each return period was analyzed to discern trends and shifts in the occurrence and intensity of compound flooding from TCs. Figure 7 (I-L) reveals that, for high-frequency events, the level of compound flooding resulting from intensified TCs and SLR will increase by 0.5-1.0 meters in coastal areas and by 2.0-2.5 meters for low-frequency events in the same regions. In inland areas, the risk of flooding from intensified rainfall associated with TCs in a warming climate will increase significantly, with flooding levels rising by 1.5-2.5 meters for low-frequency intensified TCs in the majority of areas.

The detailed, granular information provided in this section regarding compound flooding in the late 20th century and in a warming climate in the late 21st century is crucial for tailoring effective adaptation strategies in infrastructure design, as well as for the construction of buildings and critical infrastructure such as power plants. This information is also important for formulating policies and structuring insurance to discourage habitation in high-risk locations. Relying solely on historical risk assessments, even when extensive information is available, as depicted in Figure 7 (A-D), is insufficient. This is because the risk of compound flooding driven by TCs in future warming decades will surpass historical risk due to changes in storm climatology and SLR (Figure 7 (E-H)). Our physics-based risk assessment methodology provides a comprehensive understanding of the compound flooding risk linked to TCs, spanning historical, current, and future scenarios. Through the comparative analysis of return periods across different temporal frames, our findings serve to inform and direct strategies for mitigating and adapting to the complex challenges presented by compound flooding in a continually evolving climate. Therefore, it is desirable to ground design decisions in physics-based risk assessment outcomes tailored to the future warming climate to establish resilience in infrastructure, urban development, and community preparedness.

Extratropical cyclones compound flooding risk in current and future climates

In Figure 8, we illustrate the contributions of ETC climatology changes and SLR to variations in the risk of compound flooding within the depicted area, encompassing both current and anticipated future warming climates. Our analysis is limited to high-frequency events, defined by return periods of 20 years or less, due to constraints associated with our downscaled dataset. The combined impact of ETC climatology changes and SLR is projected to lead to a nearly threefold increase in the likelihood of compound flooding by the end of the century in the selected coastal area. Specifically, compound flooding events with high-frequency occurrences, with a 5% annual probability, are expected to occur with a 14% annual likelihood by the end of the century. These pronounced changes are primarily observed in the coastal areas.

To gain deeper insights into the effects of ETC climatology change and SLR, we also quantify the spatially varying risk of compound flooding events in the current and future warming climate. Figures 9 (A-D) depict the results for the current climate, while Figures 9 (E-H) display the projections for the end of the century. In Figures 9 (I-L), we highlight differences in flooding levels across different regions for the specified return periods. Evidently, coastal areas exhibit a pronounced intensification of compound flooding, attributed primarily to SLR within these regions. The magnitude of this intensification in compound flooding levels increases from events with return periods of 2 years to those with return periods of 20 years. However, unlike TC-driven compound flooding, the levels of flooding resulting from ETC events in inland areas display a distinct pattern for high-frequency ETC events. Our findings indicate no discernible trend in terms of flooding levels in inland areas at the end of the 21st century, relative to the current climate. In fact, some areas even exhibit a decreasing trend, with only some low-lying regions displaying an increasing trend, which is not statistically significant when compared to the current climate. Therefore, our results suggest that rainfall-driven flooding from high-frequency ETC events will not intensify in inland areas from future ETC events relative to the ones in the current climate. The bulk of the intensification is expected to occur along coastal areas, driven primarily by SLR during high-frequency ETC events. These findings align with prior studies (Lin et al., 2019; Booth et al., 2021), which indicate that the effects of climate change on ETC storms are relatively minor compared to the significant impact of SLR on storm surge intensification in northeastern U.S. coastal areas. To enhance our understanding and facilitate comparisons, it is imperative to include more dynamically downscaled ETC events over longer time periods, particularly focusing on low-frequency events. This would allow us to comprehensively assess the risk of compound flooding associated with these low-frequency ETC events, similar to the approach taken in our analysis of TC-driven compound flooding events.

4 Conclusion

In this study, we employed a physics-based risk assessment methodology designed to quantify the risk of compound flooding stemming from tropical and extratropical cyclones in coastal regions. We emphasize the virtues of a physics-based approach, which circumvents the severe limitations of historically based assessments, given the shortness of the records and the growing irrelevance of history in a changing climate. Such methods are essential for understanding the evolving landscape of compound flooding risk in coastal areas within the current and future climates. Our methodology offers a comprehensive means of assessing past, present, and future risks under the influence of changing storm drivers and SLR, which amplifies coastal flooding.

To achieve our objectives, we employed a two-pronged approach. First, we downscaled from reanalyses and climate models comprehensive datasets of synthetic TCs using a statistical-deterministic method. Additionally, we downscaled ETCs using WRF. These simulations were informed by key climate statistics and reanalysis data, addressing the challenges associated with the scarcity of relevant datasets over varying time periods. Furthermore, this approach allowed us to account for the influence of climate change on the primary drivers of compound flooding. In order to quantify the risk of compound flooding, our methodology explicitly considers the intricate hydrodynamics of this phenomenon. It takes into account the simultaneous interplay of surge-driven and rainfall-driven flooding across time and space during the landfall of each storm. This unique approach enables us to assess the contribution and magnitude of primary drivers, such as rainfall intensity, wind speed, and SLR, in amplifying compound flooding and backwater effects across both time and space at high resolution. It also facilitates the assessment of the contribution of each individual flooding type to the overall compound flooding risk assessment. Our results underscore the underestimation of both individual flooding hazards and the overall risk of compound flooding stemming from both TCs and ETCs, particularly in a warming climate. This underscores the significance of using numerical simulations that incorporate the complex hydrodynamics of explicit compound flooding caused by TCs and ETCs. This approach emphasizes the importance of moving away from reliance solely on statistical joint distribution of the drivers of compound flooding or conventional statistical or physical methods that focus exclusively on individual drivers or hazards (Gori et al., 2022; Moftakhari et al., 2017; Lin et al., 2019, 2016; Garner et al., 2017; Reed et al., 2015).

Our methodology is instrumental for understanding the contribution of storm climatology changes and SLR to the evolution of compound flooding risk over time. We find that TC-driven compound flooding risk is considerably higher than that of ETC-driven events, especially for high-frequency events in the Buzzards Bay area. Our results further demonstrate an increased risk of TC-driven compound flooding in the present climate compared to the late 20th century, with significant intensification anticipated in future warming climates. SLR emerges as a substantial contributor to this heightened risk. In the case of high-frequency ETC-driven compound flooding, we anticipate an amplified risk in coastal areas by the end of the century, primarily due to SLR. Nevertheless, the risk in inland areas seems to remain relatively stable, with specific regions even experiencing a reduced risk of rainfall-driven flooding.

While our methodology excels at assessing risk associated with rare events, its capacity to evaluate ETC-driven risk is limited by the scarcity of events feasible for simulation using three-dimensional models like WRF. Future research should focus on more efficient methods for downscaling ETC storms, potentially through high-resolution global model ensembles in present and future climates. Though our study did not address the interaction of astronomical tides with storm surge and SLR, we acknowledge their importance and recommend their inclusion in future assessments of surge and compound flood hazards. Our methodology can be extended beyond the Buzzards Bay area and New York City (Sarhadi et al., 2024) and can be applied as a scalable framework for vulnerable coastal regions worldwide that face the imminent threat of compound flooding from TCs and ETCs, even in the absence of historical records, regardless of their latitude. However, it is essential to tailor the methodology to incorporate region-specific factors, such as bathymetry, soil characteristics, coastal morphology, storm surge dynamics, and tidal influences. Customization helps ensure the accurate assessment and quantification of the compound flooding hazard by tailoring the approach to the specific characteristics and conditions of the region or scenario.

Our methodology also equips decision-makers with scientifically-informed insights to enhance preparedness and resilience of coastal areas. It enables authorities to estimate the likelihood of destructive storms in both current and future decades and quantify potential damages. Regional assessments empower authorities to customize adaptation strategies, allocate resources effectively, and safeguard critical infrastructure and coastal communities. Our study can serve as a cornerstone for proactive risk assessment, especially given the projected population increase within flood-prone coastal zones and megacities by 2050 (Aerts et al., 2014; Neumann et al., 2015; Kulp & Strauss, 2019). Notably, despite the significant assets in coastal flood-prone areas, investments in protective measures often fall short. Our methodology provides a comprehensive guide to ensure that adaptation efforts are precisely tailored to address the unique challenges posed by compound flooding in coastal cities. In addition to localized adaptation measures, the need to reduce greenhouse gas emissions takes center stage in mitigating the increased risk and reducing associated damages within a warming climate.

In summary, our research significantly advances our comprehension of the multi-faceted risks associated with compound flooding, while concurrently providing decision-makers with a robust analytical framework and requisite resources to fortify the resilience of vulnerable coastal regions in response to the escalating influence of climate change. Consequently, our study can serve as an essential foundation for the development and implementation of comprehensive strategies encompassing damage mitigation, strategic design, anticipatory planning, predictive forecasting, adaptive measures, and proactive mitigation interventions, all specifically tailored to address the complexities of coastal flooding caused by cyclonic storms.

Acknowledgments

The authors express their gratitude to Muge Komurcu, Matthew Huber, and Stanley Glidden for providing WRF dynamical downscaling data for ETC events. We also acknowledge the World Climate Research Programme, which, through its Working Group on Coupled Modelling, coordinated and promoted CMIP. We thank the climate modeling groups, including CESM2, CNRM-ESM2-1, EC-EARTH3, IPSL-CM6A-LR, MIROC6, and UKESM1-0-LL for producing and making available their model output. Financial support for this work was provided by Homesite Insurance.

Data availability statement

For surge modeling, historical SLR data in the study area were obtained from NOAA (`https://www.tidesandcurrents.noaa.gov/sltrends/`). The CMIP6 SLR projections under the SSP3-7.0 scenario are also available at `https://sealevel.nasa.gov/ipcc-ar6-sea-level-projection-tool?psmsl\_id=12`. Additional data utilized in flood modeling, such as current bathymetry and coastal features, can be obtained from the following source, `https://www.ncei.noaa.gov/maps/bathymetry/`. The LiDAR-based Digital Elevation Model (DEM) with a computationally feasible spatial resolution of ~ 20 m to represent the topography of the area is available at `https://coast.noaa.gov/dataviewer/`. The landuse map to quantify surface roughness is accessible at `https://www.mrlc.gov/`. A map showing soil available water storage, which is used to assess top-soil infiltration rates, can be found at `https://websoilsurvey.sc.egov.usda.gov/`. Synthetic TC tracks are based on the methodology described by Emanuel et al. (2006), and ETC event data are available from Komurcu et al. (2018).

References

Aerts, J. C., Botzen, W. W., Emanuel, K., Lin, N., De Moel, H., & Michel-Kerjan, E. O. (2014). Evaluating flood resilience strategies for coastal megacities. *Science*, *344*(6183), 473–475.

Bakkensen, L. A., & Mendelsohn, R. O. (2019). Global tropical cyclone damages and fatalities under climate change: An updated assessment. *Hurricane risk*, 179–197.

Bates, P. D., Horritt, M. S., & Fewtrell, T. J. (2010). A simple inertial formulation of the shallow water equations for efficient two-dimensional flood inundation modelling. *Journal of Hydrology*, *387*(1-2), 33–45.

Bates, P. D., Quinn, N., Sampson, C., Smith, A., Wing, O., Sosa, J., ... others (2021). Combined modeling of us fluvial, pluvial, and coastal flood hazard under current and future climates. *Water Resources Research*, *57*(2), e2020WR028673.

Berger, M. J., George, D. L., LeVeque, R. J., & Mandli, K. T. (2011). The geoclaw software for depth-averaged flows with adaptive refinement. *Advances in Water Resources*, *34*(9), 1195–1206.

Booth, J. F., Narinesingh, V., Towey, K. L., & Jeyaratnam, J. (2021). Storm surge, blocking, and cyclones: A compound hazards analysis for the northeast united states. *Journal of Applied Meteorology and Climatology*, *60*(11), 1531–1544.

Colle, B. A., Booth, J. F., & Chang, E. K. (2015). A review of historical and future changes of extratropical cyclones and associated impacts along the us east coast. *Current Climate Change Reports*, *1*, 125–143.

Colle, B. A., Buonaiuto, F., Bowman, M. J., Wilson, R. E., Flood, R., Hunter, R., ... Hill, D. (2008). New york city's vulnerability to coastal flooding: Storm surge modeling of past cyclones. *Bulletin of the American Meteorological Society*, *89*(6), 829–842.

Dee, D. P., Uppala, S. M., Simmons, A. J., Berrisford, P., Poli, P., Kobayashi, S., ... others (2011). The era-interim reanalysis: Configuration and performance of the data assimilation system. *Quarterly Journal of the royal meteorological society*, *137*(656), 553–597.

Emanuel, K. (2017). Assessing the present and future probability of hurricane harvey's rainfall. *Proceedings of the National Academy of Sciences*, *114*(48), 12681–12684.

Emanuel, K., DesAutels, C., Holloway, C., & Korty, R. (2004). Environmental control of tropical cyclone intensity. *Journal of the atmospheric sciences*, *61*(7), 843–858.

Emanuel, K., Ravela, S., Vivant, E., & Risi, C. (2006). A statistical deterministic approach to hurricane risk assessment. *Bulletin of the American Meteorological Society*, *87*(3), 299–314.

Emanuel, K., Sundararajan, R., & Williams, J. (2008). Hurricanes and global warming: Results from downscaling ipcc ar4 simulations. *Bulletin of the American Meteorological Society*, *89*(3), 347–368.

Feldmann, M., Emanuel, K., Zhu, L., & Lohmann, U. (2019). Estimation of atlantic tropical cyclone rainfall frequency in the united states. *Journal of Applied Meteorology and Climatology*, *58*(8), 1853–1866.

Fox-Kemper, B., Hewitt, H., Xiao, C., Aalgeirsdóttir, G., Drijfhout, S., Edwards, T., ... others (2021). Ocean, cryosphere and sea level change.

Garner, A. J., Mann, M. E., Emanuel, K. A., Kopp, R. E., Lin, N., Alley, R. B., ... Pollard, D. (2017). Impact of climate change on new york city's coastal flood hazard: Increasing flood heights from the preindustrial to 2300 ce. *Proceedings of the National Academy of Sciences*, *114*(45), 11861–11866.

Gori, A., & Lin, N. (2022). Projecting compound flood hazard under climate change with physical models and joint probability methods. *Earth's Future*, *10*(12), e2022EF003097.

Gori, A., Lin, N., & Smith, J. (2020). Assessing compound flooding from landfalling tropical cyclones on the north carolina coast. *Water Resources Research*, *56*(4), e2019WR026788.

Gori, A., Lin, N., Xi, D., & Emanuel, K. (2022). Tropical cyclone climatology change greatly exacerbates us extreme rainfall–surge hazard. *Nature Climate Change*, *12*(2), 171–178.

Komurcu, M., Emanuel, K., Huber, M., & Acosta, R. (2018). High-resolution climate projections for the northeastern united states using dynamical downscaling at convection-permitting scales. *Earth and Space Science*, *5*(11), 801–826.

Kossin, J. P. (2018). A global slowdown of tropical-cyclone translation speed. *Nature*, *558*(7708), 104–107.

Kossin, J. P., Emanuel, K. A., & Vecchi, G. A. (2014). The poleward migration of the location of tropical cyclone maximum intensity. *Nature*, *509*(7500), 349–352.

Kulp, S. A., & Strauss, B. H. (2019). New elevation data triple estimates of global vulnerability to sea-level rise and coastal flooding. *Nature communications*, *10*(1), 1–12.

Lin, N., Emanuel, K., Oppenheimer, M., & Vanmarcke, E. (2012). Physically based assessment of hurricane surge threat under climate change. *Nature Climate Change*, *2*(6), 462–467.

Lin, N., Kopp, R. E., Horton, B. P., & Donnelly, J. P. (2016). Hurricane sandy's flood frequency increasing from year 1800 to 2100. *Proceedings of the National Academy of Sciences*, *113*(43), 12071–12075.

Lin, N., Marsooli, R., & Colle, B. A. (2019). Storm surge return levels induced by mid-to-late-twenty-first-century extratropical cyclones in the northeastern united states. *Climatic change*, *154*, 143–158.

Liu, M., Vecchi, G. A., Smith, J. A., & Knutson, T. R. (2019). Causes of large projected increases in hurricane precipitation rates with global warming. *NPJ climate and atmospheric science*, *2*(1), 38.

Mandli, K. T., & Dawson, C. N. (2014). Adaptive mesh refinement for storm surge. *Ocean Modelling*, *75*, 36–50.

Marsooli, R., Lin, N., Emanuel, K., & Feng, K. (2019). Climate change exacerbates hurricane flood hazards along us atlantic and gulf coasts in spatially varying patterns. *Nature communications*, *10*(1), 1–9.

Miura, Y., Mandli, K. T., & Deodatis, G. (2021). High-speed gis-based simulation of storm surge–induced flooding accounting for sea level rise. *Natural Hazards Review*, *22*(3), 04021018.

Moftakhari, H. R., Salvadori, G., AghaKouchak, A., Sanders, B. F., & Matthew, R. A. (2017). Compounding effects of sea level rise and fluvial flooding. *Proceedings of the National Academy of Sciences*, *114*(37), 9785–9790.

Müller, M. (2011). Rapid change in semi-diurnal tides in the north atlantic since 1980. *Geophysical research letters*, *38*(11).

Neal, J., Schumann, G., & Bates, P. (2012). A subgrid channel model for simulating river hydraulics and floodplain inundation over large and data sparse areas. *Water Resources Research*, *48*(11).

Neumann, B., Vafeidis, A. T., Zimmermann, J., & Nicholls, R. J. (2015). Future coastal population growth and exposure to sea-level rise and coastal flooding-a global assessment. *PloS one*, *10*(3), e0118571.

Reed, A. J., Mann, M. E., Emanuel, K. A., Lin, N., Horton, B. P., Kemp, A. C., & Donnelly, J. P. (2015). Increased threat of tropical cyclones and coastal flooding to new york city during the anthropogenic era. *Proceedings of the National Academy of Sciences*, *112*(41), 12610–12615.

Sarhadi, A., Rousseau-Rizzi, R., Mandli, K., Neal, J., Wiper, M. P., Feldmann, M., & Emanuel, K. (2024). Climate change contributions to increasing compound flooding risk in new york city. *Bulletin of the American Meteorological Society*.

Strauss, B. H., Orton, P. M., Bittermann, K., Buchanan, M. K., Gilford, D. M., Kopp, R. E., … Vinogradov, S. (2021). Economic damages from hurricane sandy attributable to sea level rise caused by anthropogenic climate change. *Nature communications*, *12*(1), 1–9.

Studholme, J., Fedorov, A. V., Gulev, S. K., Emanuel, K., & Hodges, K. (2022). Poleward expansion of tropical cyclone latitudes in warming climates. *Nature Geoscience*, *15*(1), 14–28.

Wahl, T., Jain, S., Bender, J., Meyers, S. D., & Luther, M. E. (2015). Increasing risk of compound flooding from storm surge and rainfall for major us cities. *Nature Climate Change*, *5*(12), 1093–1097.

Westerink, J. J., Luettich, R. A., Feyen, J. C., Atkinson, J. H., Dawson, C., Roberts, H. J., … Pourtaheri, H. (2008). A basin-to channel-scale unstructured grid hurricane storm surge model applied to southern louisiana. *Monthly weather*

review, *136* (3), 833–864.
Wing, O. E., Lehman, W., Bates, P. D., Sampson, C. C., Quinn, N., Smith, A. M., ... Kousky, C. (2022). Inequitable patterns of us flood risk in the anthropocene. *Nature Climate Change*, *12* (2), 156–162.
Xi, D., Lin, N., & Smith, J. (2020). Evaluation of a physics-based tropical cyclone rainfall model for risk assessment. *Journal of Hydrometeorology*, *21* (9), 2197–2218.
Zhang, Y., & Najafi, M. R. (2020). Probabilistic numerical modeling of compound flooding caused by tropical storm matthew over a data-scarce coastal environment. *Water Resources Research*, *56* (10), e2020WR028565.

Figure 1. Surge simulation process for ETCs using dynamically downscaled WRF simulations of primary drivers (wind speed and sea level pressure fields) in the study area. (A) Three nested grids with spatial resolutions of 27, 9, and 3-km used for dynamically downscaling WRF simulations (in this study, we focus on the 3-km spatial resolution domain). (B-C) Hourly wind and pressure fields downscaled via WRF simulations driven by ERA-Interim reanalysis for an ETC event occurred on 27-28th December 2012. (D) Simulated surge height (in meters) from the ETC at the regional scale using modified GeoClaw. (E) Performance evaluation of GeoClaw for the ETC storm (the blue line represents observed surge heights during the landfall of the ETCs, calculated by de-tiding water levels, with water elevation subtracted from NOAA tide predictions at the Woods Hole gauge. The red line represents surge heights simulated by GeoClaw. Note that the temporal resolution on the x-axis is six minutes).

Figure 2. Impact of key drivers of compound flooding, such as rainfall intensity and surface wind speed. The top panels include the Probability Distribution Function of rainfall intensity (mm/hr) at each grid cell during landfall and the maximum surface wind speed (knots) at the eye of synthetic TC tracks, both before and at the time of landfall, for two selected synthetic TCs in the current climate downscaled by NCEP reanalysis data. The lower panels depict the corresponding compound flooding response for the two synthetic TCs. (A and B) show the drivers and compound flooding for TC track 1337, while (C and D) show the same results for synthetic TC track 1339.

Figure 3. Comparison of compound flooding risk assessment relative to individual surge and rainfall-driven flooding, and linear addition of individual hazards. (A) Maximum compound flooding level from a randomly selected synthetic TC generated from the EC-EARTH3 model during the late 20th century, along with the location of a coastal area chosen for comparing different types of flooding. (B-C) Flooding levels as a function of the return period from various individual and compound flooding hazard sources for the selected coastal area, using synthetic TCs generated from the CESM2 model for the late 20th and 21st centuries, respectively. (D-M) Similar to (B-C) but using synthetic TCs generated from other climate models. The shaded areas in the plots represent sampling uncertainty bounds, calculated based on the 5th and 95th percentiles of a Poisson distribution within each climate model.

Figure 4. Assessment of the contribution of SLR and changes in TC climatology to the risk of compound flooding in the late 20th and 21st centuries, focusing on the selected location depicted in Figure 3 (A). Each line in the graph illustrates the simulated compound flooding levels derived from synthetic TCs downscaled from each of the six climate models. The shaded region represents the confidence interval, indicating sampling uncertainty, and is calculated based on the 5th and 95th percentiles of a Poisson distribution within each climate model.

Figure 5. Impact of TC climatology change and SLR on the alteration of compound flooding risk during today's climate (2000-2020) in comparison to the late 20th century (1979-1999) in a selected coastal location. (A) representation of the compound flooding levels as a function of return period, comparing today's climate with the late 20th century. The results are derived from the depicted coastal location, excluding intertidal zones. Each line represents compound flooding outcomes produced through the generation of synthetic TCs based on reanalysis NCEP data for the respective time periods. The shaded areas in the figure indicate the sampling uncertainty margins, calculated using the 5th and 95th percentiles of a Poisson distribution. (B) Assessment of the impact of changes in TC climatology and SLR on the spatially-varying risk of 100-year return period compound flooding events in today's climate relative to the late 20th century. In this map, red color denotes an increasing trend, blue color represents a decreasing trend, and gray color signifies areas exhibiting no discernible trend or values close to zero.

Figure 6. Impact of TC climatology changes and SLR on compound flooding in historical, present, and future climates in the selected coastal area (depicted in the left panels). Each line represents the outcomes derived from synthetic TCs downscaled from multiple climate models and reanalysis data for the three timeframes: historical (dark blue), present (light blue), and future climates (red). The shading in the figure represents confidence intervals (5% and 95%) derived through a bootstrapping approach for the ensemble of climate models. See text for details.

Figure 7. Spatially distributed granular risk of compound flooding from TCs in past and future climates. (A-D) Present the results of compound flooding for various return periods in the late 20th century. (E-H) Depict the same analysis for the late 21st century. (I-L) Illustrate the differences in compound flooding levels between the late 21st century and late 20th century for different return periods. Here, red indicates an increasing trend, blue indicates a decreasing trend, and gray signifies no clear trend or values close to zero. Note that these results are based on the ensemble mean of the six CMIP6 climate models.

Figure 8. Impact of ETC climatology changes and SLR on the risk of compound flooding in the current and future climates in the selected coastal area (depicted in the left panels). Each line represents the outcomes derived from dynamically downscaled ETC events for two timeframes: the current climate (2006-2020, shown in blue) and future climates (2081-2100, shown in red). The shading in the figure represents confidence intervals (5% and 95%) derived through a bootstrapping approach.

Figure 9. Spatially distributed granular risk of compound flooding from ETCs in the current and future climates. (A-D) Present the results of compound flooding for various return periods in the current climate. (E-H) Depict the same analysis for the late 21st century. (I-L) Illustrate the differences in compound flooding levels between the late 21st century and the current climate for various return periods. Note that red indicates an increasing trend, blue indicates a decreasing trend, and gray signifies no clear trend or values close to zero.

Figure 1.

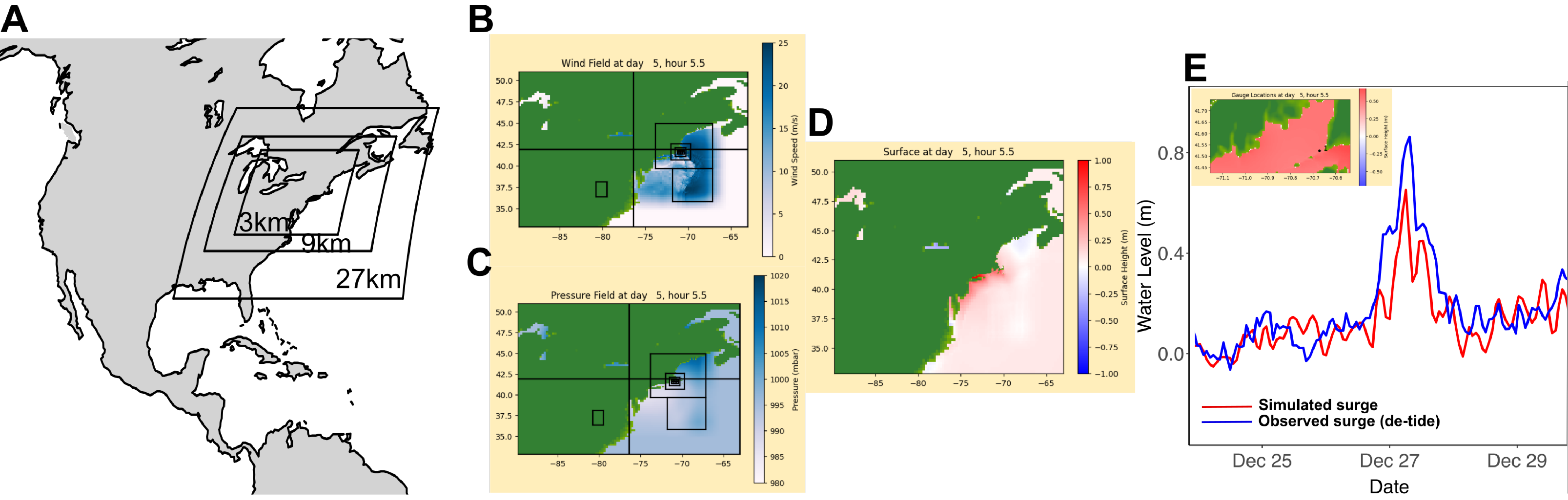

A
3km
9km
27km
B
Wind Field at day 5, hour 5.5
Wind Speed (m/s)
C
Pressure Field at day 5, hour 5.5
Pressure (mbar)
D
Surface at day 5, hour 5.5
Surface Height (m)
E
Gauge Locations at day 5, hour 5.5
Water Level (m)
Simulated surge
Observed surge (de-tide)
Dec 25
Dec 27
Dec 29
Date

Figure 2.

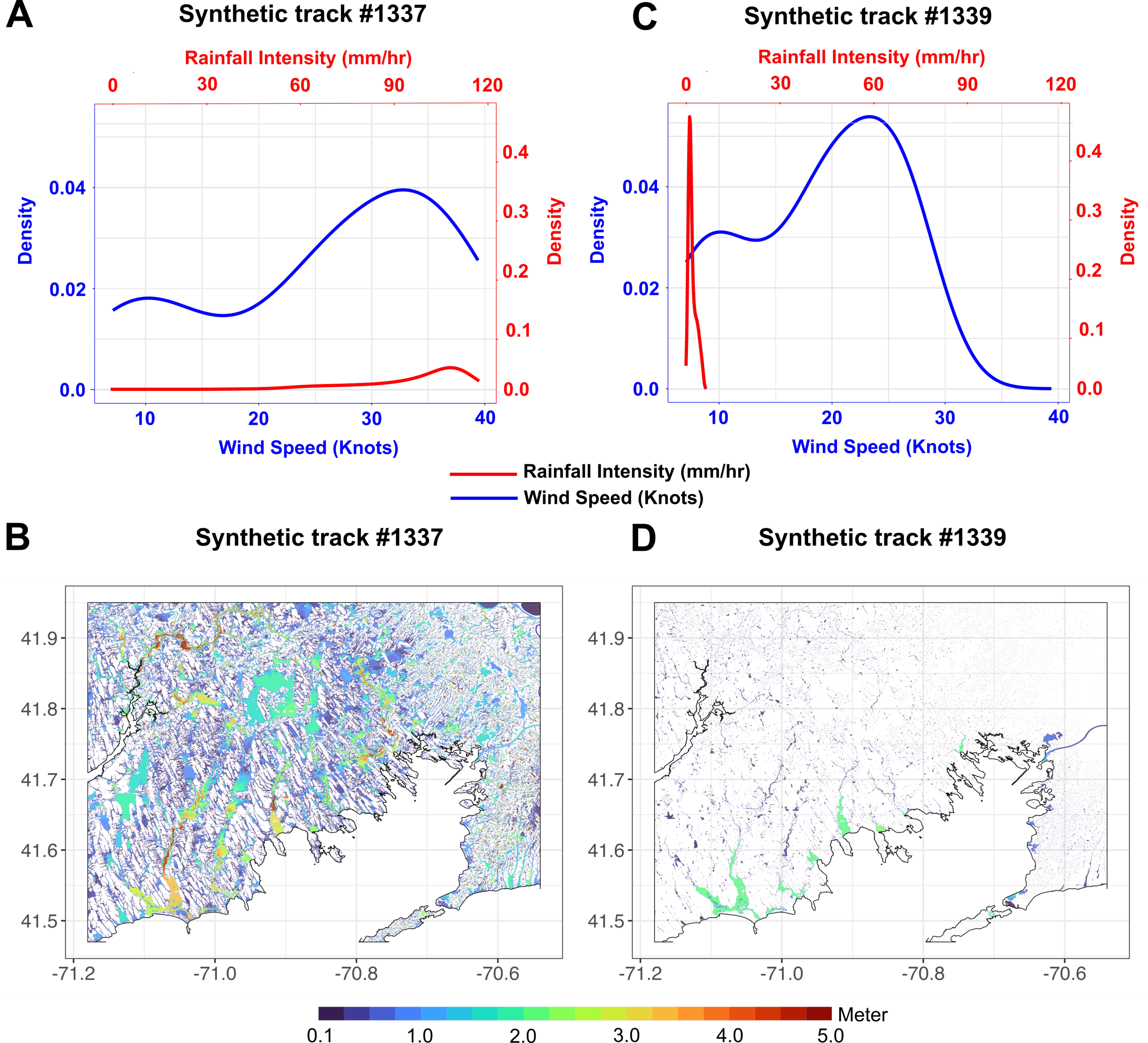
A
Synthetic track #1337
Rainfall Intensity (mm/hr)
0
30
60
90
120
Density
0.04
0.02
0.0
0.4
0.3
0.2
0.1
0.0
Density
10
20
30
40
Wind Speed (Knots)
C
Synthetic track #1339
Rainfall Intensity (mm/hr)
0
30
60
90
120
Density
0.04
0.02
0.0
0.4
0.3
0.2
0.1
0.0
Density
10
20
30
40
Wind Speed (Knots)
Rainfall Intensity (mm/hr)
Wind Speed (Knots)
B
Synthetic track #1337
41.9
41.8
41.7
41.6
41.5
-71.2
-71.0
-70.8
-70.6
D
Synthetic track #1339
41.9
41.8
41.7
41.6
41.5
-71.2
-71.0
-70.8
-70.6
0.1
1.0
2.0
3.0
4.0
5.0
Meter

Figure 3.

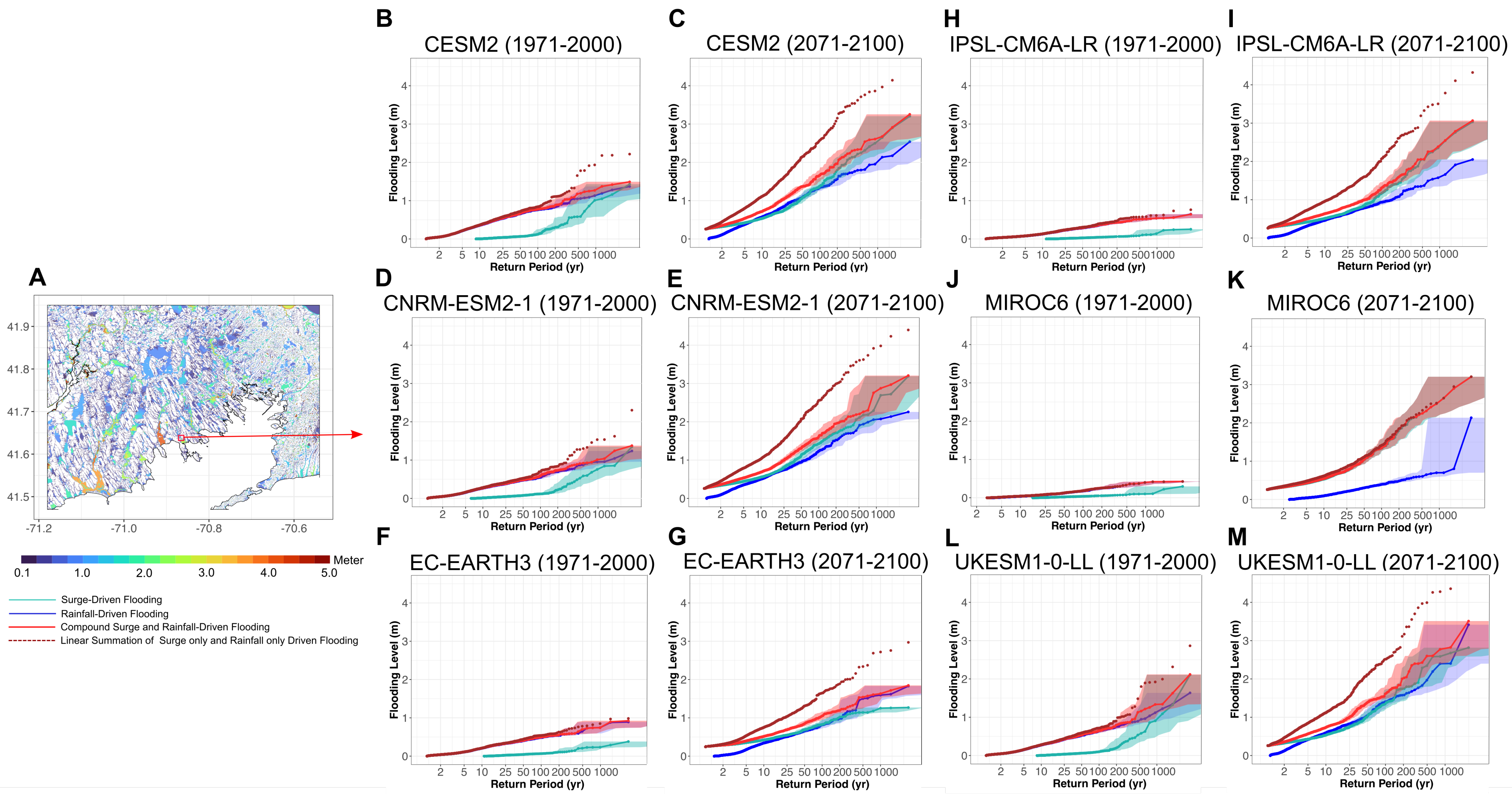

A
B
CESM2 (1971-2000)
C
CESM2 (2071-2100)
D
CNRM-ESM2-1 (1971-2000)
E
CNRM-ESM2-1 (2071-2100)
F
EC-EARTH3 (1971-2000)
G
EC-EARTH3 (2071-2100)
H
IPSL-CM6A-LR (1971-2000)
I
IPSL-CM6A-LR (2071-2100)
J
MIROC6 (1971-2000)
K
MIROC6 (2071-2100)
L
UKESM1-0-LL (1971-2000)
M
UKESM1-0-LL (2071-2100)
Flooding Level (m)
Return Period (yr)
Meter
0.1 1.0 2.0 3.0 4.0 5.0
Surge-Driven Flooding
Rainfall-Driven Flooding
Compound Surge and Rainfall-Driven Flooding
Linear Summation of Surge only and Rainfall only Driven Flooding

Figure 4.

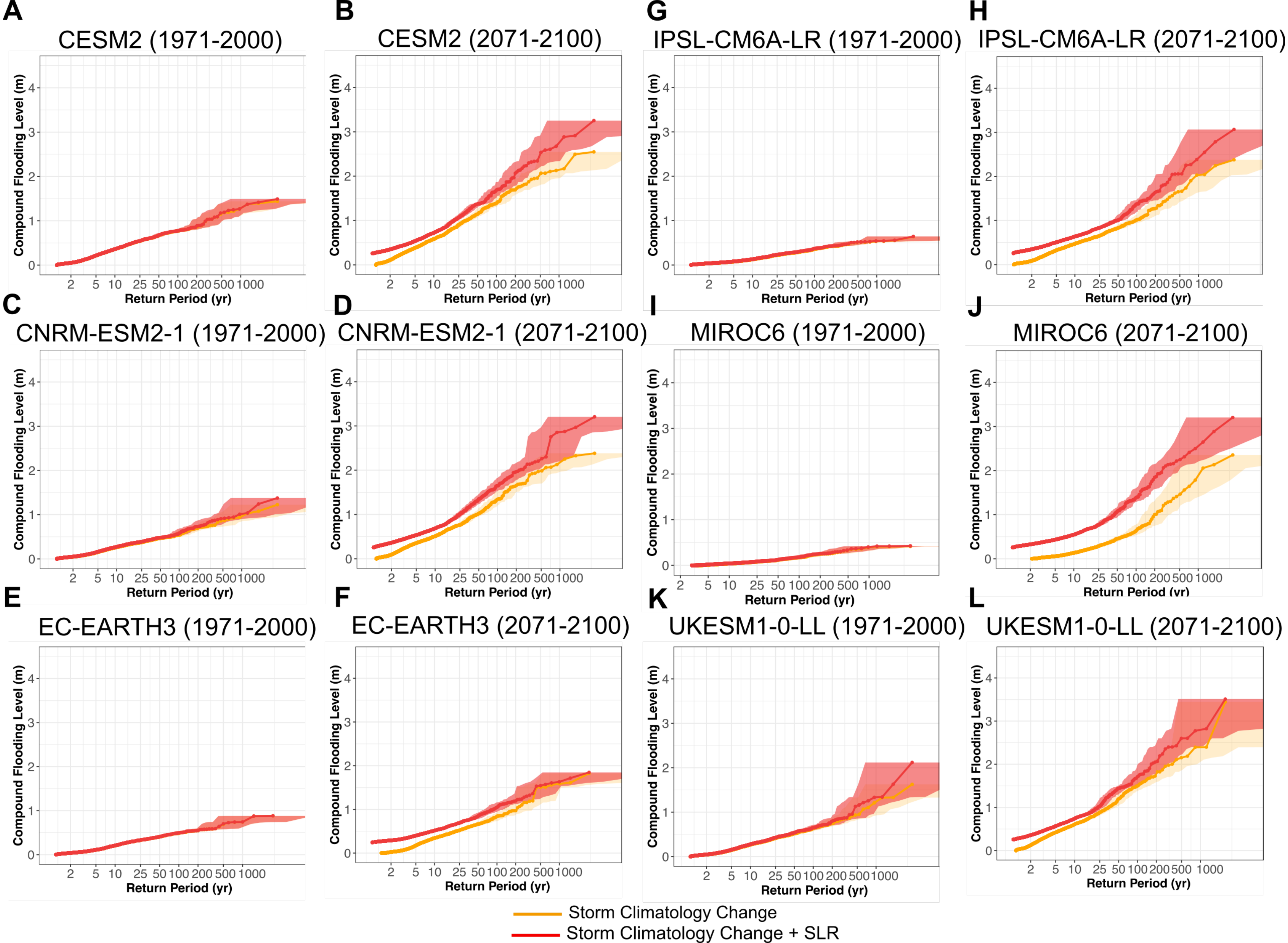

A
CESM2 (1971-2000)
B
CESM2 (2071-2100)
G
IPSL-CM6A-LR (1971-2000)
H
IPSL-CM6A-LR (2071-2100)
C
CNRM-ESM2-1 (1971-2000)
D
CNRM-ESM2-1 (2071-2100)
I
MIROC6 (1971-2000)
J
MIROC6 (2071-2100)
E
EC-EARTH3 (1971-2000)
F
EC-EARTH3 (2071-2100)
K
UKESM1-0-LL (1971-2000)
L
UKESM1-0-LL (2071-2100)
Compound Flooding Level (m)
Return Period (yr)
0
1
2
3
4
2
5
10
25
50
100
200
500
1000
Storm Climatology Change
Storm Climatology Change + SLR

Figure 5.

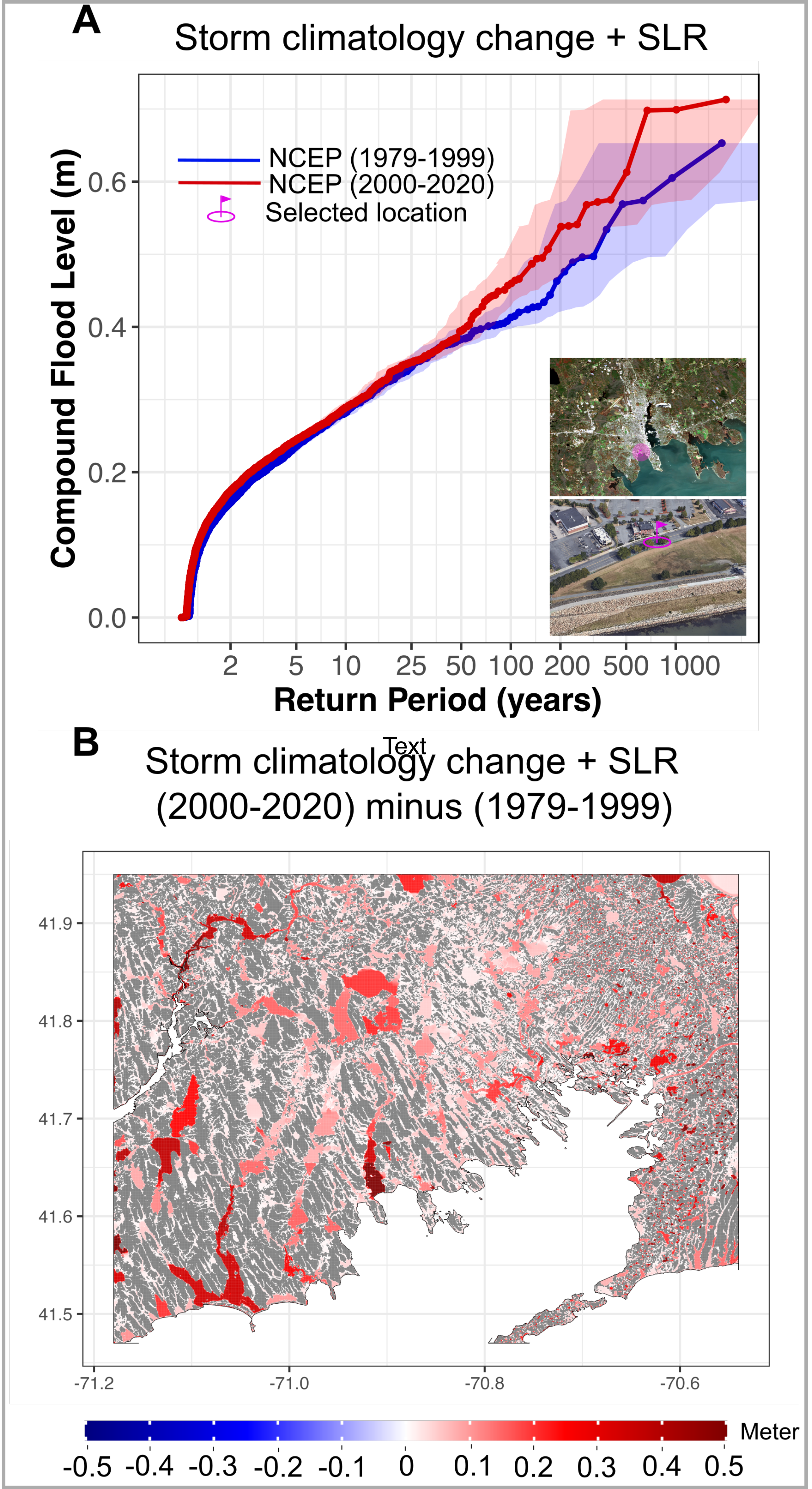
A
Storm climatology change + SLR
NCEP (1979-1999)
NCEP (2000-2020)
Selected location
Compound Flood Level (m)
0.0
0.2
0.4
0.6
2
5
10
25
50
100
200
500
1000
Return Period (years)
B
Text
Storm climatology change + SLR
(2000-2020) minus (1979-1999)
41.9
41.8
41.7
41.6
41.5
-71.2
-71.0
-70.8
-70.6
Meter
-0.5
-0.4
-0.3
-0.2
-0.1
0
0.1
0.2
0.3
0.4
0.5

Figure 6.

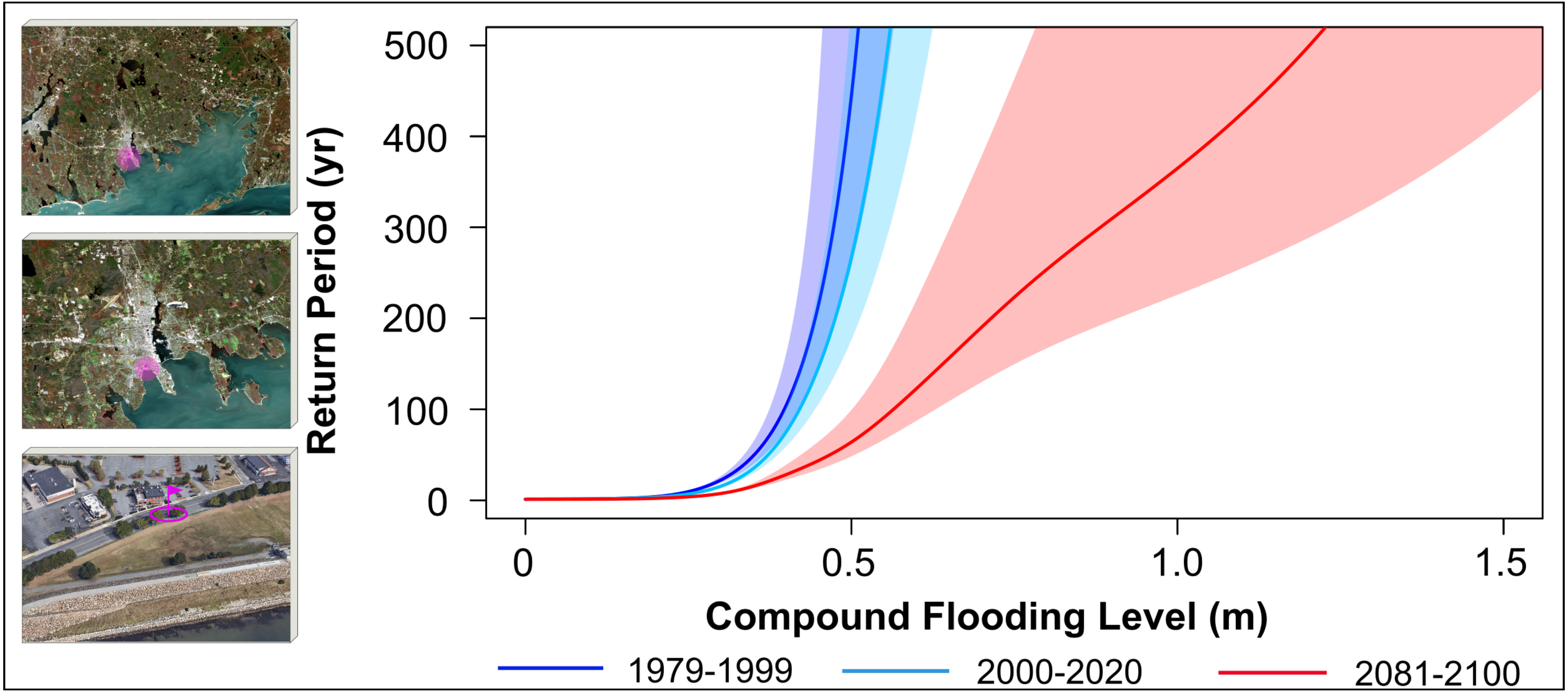
Return Period (yr)
500
400
300
200
100
0
0
0.5
1.0
1.5
Compound Flooding Level (m)
1979-1999
2000-2020
2081-2100

Figure 7.

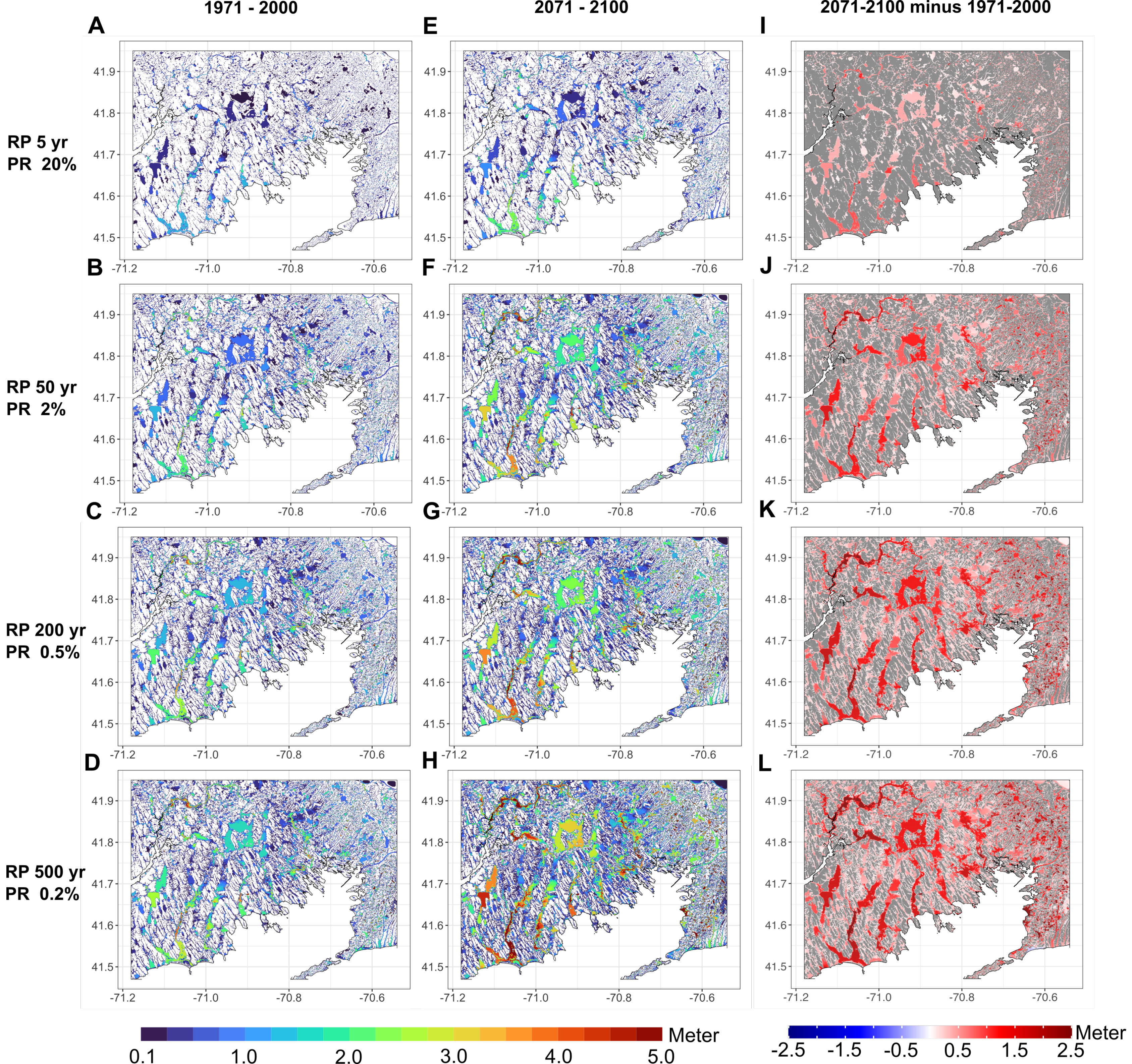

1971 - 2000
2071 - 2100
2071-2100 minus 1971-2000
A
B
C
D
E
F
G
H
I
J
K
L
RP 5 yr
PR 20%
RP 50 yr
PR 2%
RP 200 yr
PR 0.5%
RP 500 yr
PR 0.2%
41.9
41.8
41.7
41.6
41.5
-71.2
-71.0
-70.8
-70.6
0.1
1.0
2.0
3.0
4.0
5.0
Meter
-2.5
-1.5
-0.5
0.5
1.5
2.5
Meter

Figure 8.

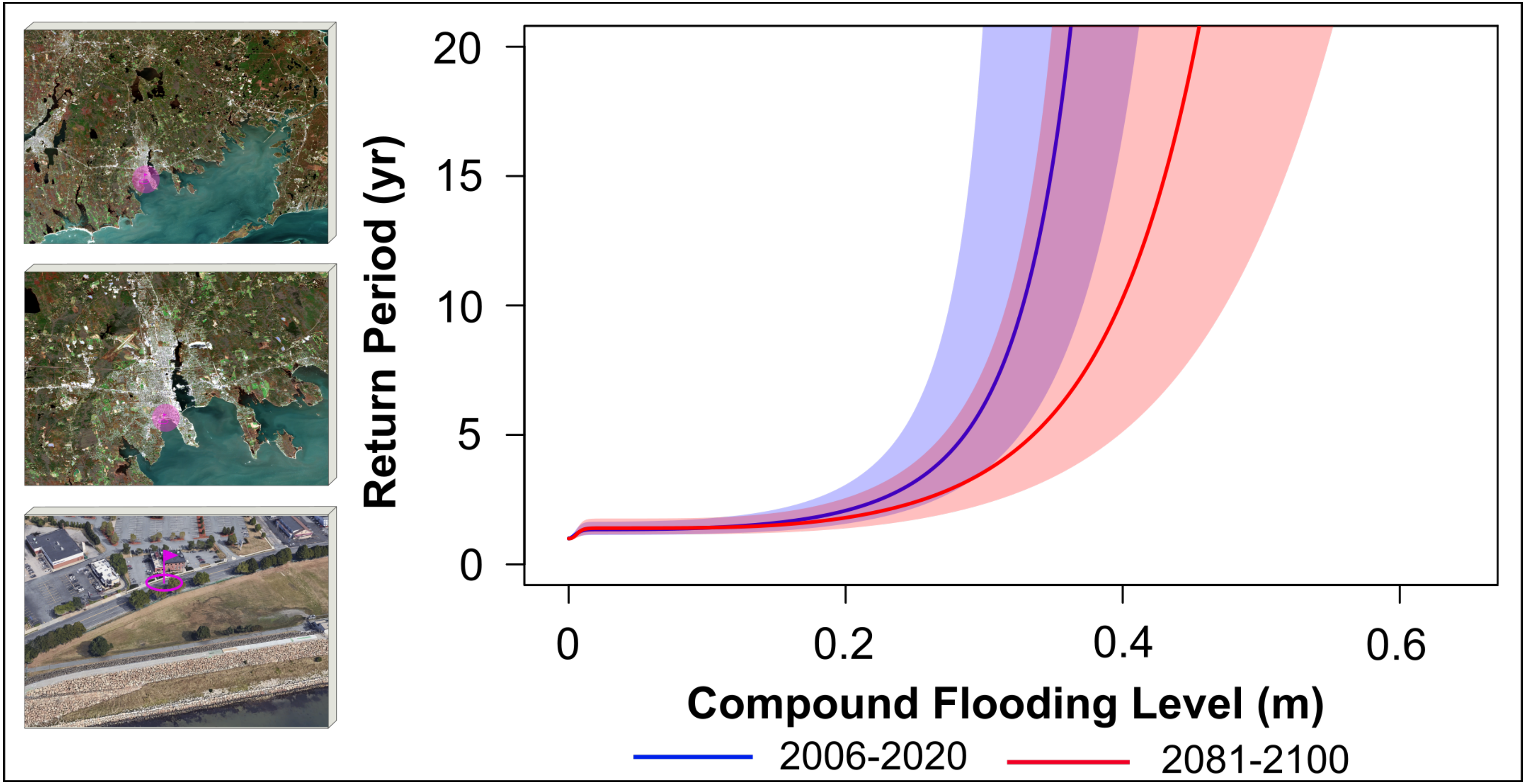

20
15
10
5
0
Return Period (yr)
0
0.2
0.4
0.6
Compound Flooding Level (m)
2006-2020
2081-2100

Figure 9.

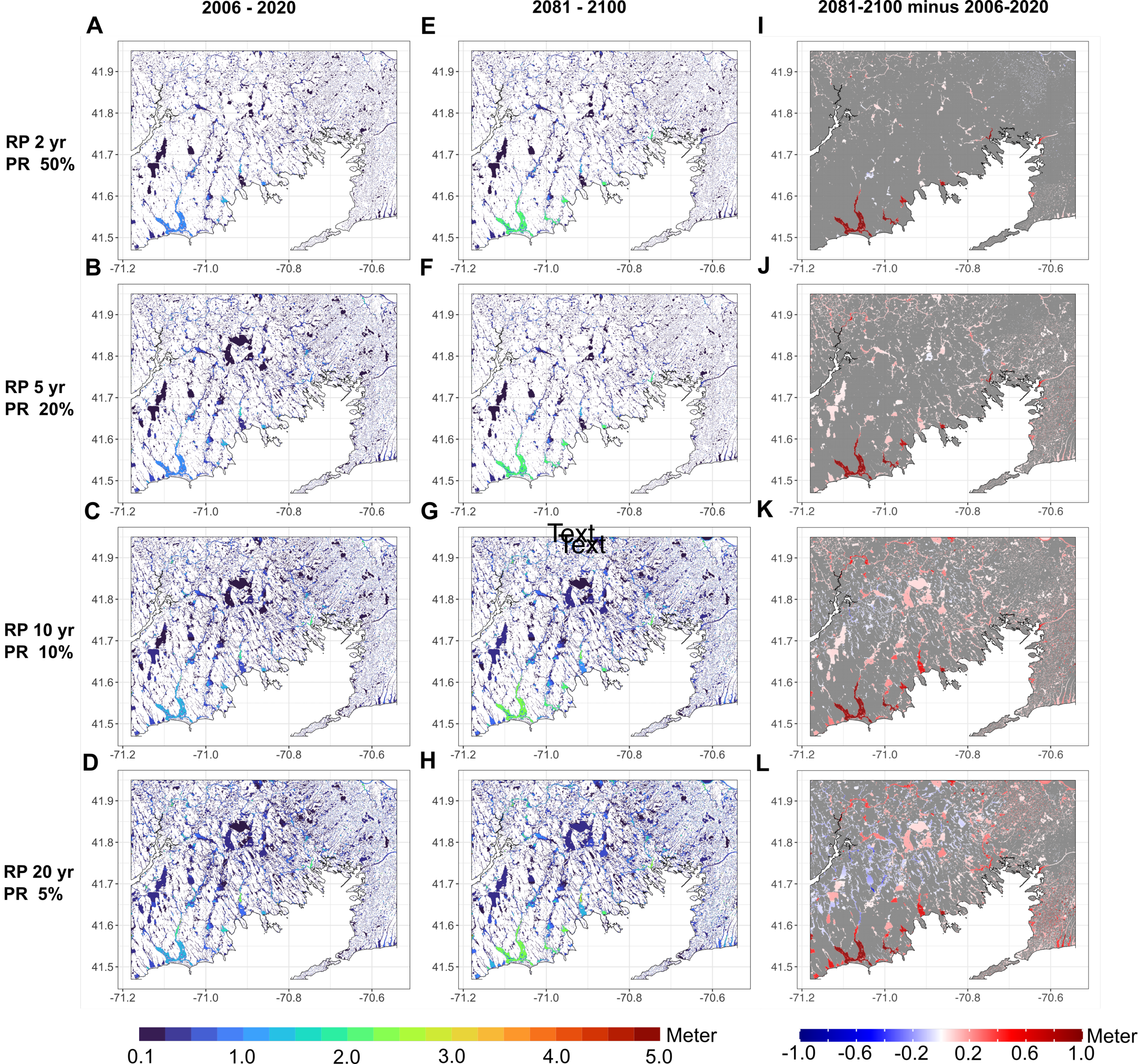
2006 - 2020
2081 - 2100
2081-2100 minus 2006-2020
A
B
C
D
E
F
G
H
I
J
K
L
RP 2 yr
PR 50%
RP 5 yr
PR 20%
RP 10 yr
PR 10%
RP 20 yr
PR 5%
41.5
41.6
41.7
41.8
41.9
-71.2
-71.0
-70.8
-70.6
Text
Text
Meter
0.1
1.0
2.0
3.0
4.0
5.0
Meter
-1.0
-0.6
-0.2
0.2
0.6
1.0

Physics-based Risk Assessment of Compound Flooding from Tropical and Extratropical Cyclones in a Warming Climate

Ali Sarhadi[1], Raphaël Rousseau-Rizzi[1], and Kerry Emanuel[1]

[1]Lorenz Center, Department of Earth Atmospheric and Planetary Sciences, Massachusetts Institute of Technology, Cambridge, MA, USA

Key Points:

- Compound flooding
- Physics-based risk modeling
- Tropical and extratropical cyclones

Corresponding author: Ali Sarhadi, `sarhadi@mit.edu`

Abstract

In recent years, efforts to assess the evolving risks of coastal compound surge and rainfall-driven flooding from tropical cyclones (TCs) and extratropical cyclones (ETCs) in a warming climate have intensified. While substantial progress has been made, the persistent challenge lies in obtaining actionable insights into the changing magnitude and spatially-varying flood risks in coastal areas. We employ a physics-based numerical hydrodynamic framework to simulate compound flooding from TCs and ETCs in both current and future warming climate conditions, focusing on the western side of Buzzard Bay in Massachusetts. Our approach leverages hydrodynamic models driven by extensive sets of synthetic TCs downscaled from CMIP6 climate models and dynamically downscaled ETC events using the WRF model forced by CMIP5 simulations. Through this methodology, we quantify the extent to which climate change can potentially reshape the risk landscape of compound flooding in the study area. Our findings reveal a significant increase in TC-induced compound flooding risk due to evolving climatology and sea level rise (SLR). Additionally, there is a heightened magnitude of compound flooding from ETCs, in coastal regions, due to SLR. Inland areas exhibit a decline in rainfall-driven flooding from high-frequency ETC events toward the end of the century compared to the current climate. Our methodology is transferable to other vulnerable coastal regions, serving as a valuable decision-making tool for adaptive measures in densely populated areas. It equips decision-makers and stakeholders with the means to effectively mitigate the destructive impacts of compound flooding arising from both current and future TCs and ETCs.

Plain Language Summary

During storms in coastal areas, strong winds can cause surge-driven flooding, and simultaneously, intense rainfall may lead to inland heavy rainfall-driven flooding. Sometimes, these two flooding sources coincide, forming compound surge and rainfall-driven flooding, which is more destructive than either hazard alone. To assess the risk of such destructive compound flooding, we use physics-based models to quantify the frequency and magnitude of these hazards. Additionally, we evaluate how climate change and factors such as sea-level rise may affect the frequency and magnitude of such events in coastal areas. Through these detailed, granular risk assessments, regions facing increased flooding threats can develop strategies to better mitigate damages posed by compound flooding during extreme storms.

1 Introduction

Tropical cyclones (TCs) are powerful storms characterized by their strong winds, heavy precipitation, and storm surges. They predominantly affect tropical coastal areas, where they can cause significant annual damage, estimated at US$26 billion in the United States alone (Bakkensen & Mendelsohn, 2019). However, recent scientific evidence indicates a notable poleward shift in TC distribution. This shift is attributed in part to global climate warming and ocean temperature rise, which create conducive conditions for the formation and propagation of TCs into higher latitudes (Kossin et al., 2014; Kossin, 2018). As TCs extend into higher latitudes, they introduce new challenges and hazards. These areas are less accustomed to such extreme weather events, and their populations, infrastructure, and ecosystems may be poorly prepared to cope with them (Studholme et al., 2022). In addition to TCs occurring during warm seasons, extratropical cyclones (ETCs) develop in cold seasons in these regions. ETCs can experience slower movement as a result of atmospheric conditions, leading to intricate storm dynamics and an elevated likelihood of causing substantial damage (Booth et al., 2021; Colle et al., 2015).

Damage resulting from TCs and ETCs is associated with various hazards inherent to these weather systems. Strong winds and the low-pressure systems accompanying these storms during landfall can induce storm surges in coastal regions, leading to coastal flooding. Subsequently, during landfall, heavy rainfall can result in inland freshwater flooding. At times, both forms of flooding can transpire simultaneously, resulting in a compound event that combines salty storm surge and freshwater rainfall-driven flooding. The intricate interplay between these two sources of flooding often results in compound flooding events that exhibit greater destructive potential compared to individual occurrences of either saltwater surge or torrential freshwater rainfall-driven flooding (Wahl et al., 2015).

In a warming climate, several factors may contribute to an increased potential for compound flooding events resulting from TCs and ETCs. It is well-established that the intensity of rainfall associated with these storms is likely to intensify. This escalation is primarily driven by higher saturation vapor pressure of water, as dictated by the Clausius-Clapeyron equation (Liu et al., 2019). Furthermore, the movement of TCs toward higher latitudes, alterations in their translational speed, and modifications in the behavior of ETCs all contribute to the altered hazards associated with these storms (Kossin, 2018; Booth et al., 2021). Additionally, the rising sea levels further exacerbate the impact of compound flooding events, necessitating a comprehensive evaluation and mitigation of the associated risks (Strauss et al., 2021; Marsooli et al., 2019; Lin et al., 2019, 2016). It is important to gain a deeper understanding of how these alterations in storm characteristics, manifesting within a future warming climate, may reshape the risk of compound flooding resulting from these storms. This is particularly vital in regions unaccustomed to such cyclonic activity, as this knowledge is essential for enhancing preparedness, facilitating adaptation, and formulating mitigation strategies aimed at reducing the potentially devastating damages associated with these events.

One significant challenge associated with TCs and ETCs is the limited availability of comprehensive records of these storms. The most reliable records we can obtain date back only to the early satellite era, starting in the 1980s. This timeframe is relatively short, and for specific regions, some landfalling storms may not have been recorded, exacerbating the issue. Consequently, when attempting to employ historical records to quantify the risk of compound flooding from these storms, a significant degree of uncertainty arises due to the brevity of the dataset and the paucity of observations. Even if more extended records of these storms were available from the past, they may not be representative of today's climate, primarily due to the influence of climate change. It is important to emphasize that even contemporary climate records do not provide an accurate representation of future conditions, again owing to ongoing climate change. Therefore, any statistical risk assessment method relying solely on historical statistics may fail to accurately quantify the risk. Infrastructure or adaptation planning based on such methodologies can thus lead to vulnerabilities and significant damages. To address this data limitation and account for the evolving climate, we employ a physics-based risk modeling framework (Sarhadi et al., 2024). This framework is driven by the atmospheric and ocean climatology of reanalysis data and General Circulation Models (GCMs) (Emanuel et al., 2006, 2008; Komurcu et al., 2018). It enables the downscaling of TCs and ETCs across past, current, and future climate scenarios. This approach helps address the dearth of observations and provides insights into how these storms may evolve under a warming climate, consequently shedding light on how the risk of compound flooding in coastal areas at higher latitudes may change.

Compound flooding arises from the complex interplay between storm surge and heavy rainfall-driven inundation, manifesting across both spatial and temporal dimensions. It is important to meticulously model this intricate hydrodynamic interaction between the two sources of flooding, distinguished by their saline (surge) and freshwater (rainfall) characteristics, with a high level of temporal and spatial precision. In recent years, there has been a growing focus on modeling intricate coastal hydrodynamics. Commonly, statistical methodologies are used to assess flood risk by establishing joint statistical distributions that capture interdependencies among various flooding drivers, often at localized or gauge scales (Gori et al., 2020; Wahl et al., 2015; Moftakhari et al., 2017; Gori & Lin, 2022; Zhang & Najafi, 2020). However, these methods have limitations, primarily stemming from their inability to account for the complex dynamic interactions between storm surge and rainfall-driven flooding. These approaches rely heavily on statistical measures of dependence, which can introduce uncertainties. Moreover, they often overlook hydraulic dynamics of compound flooding, which involves integrating surge height and rainfall intensity to determine flooding levels while considering their compounded effects. The prevailing statistical practices, which often treat the drivers of compound flooding (rainfall intensity and surge height) through joint distributions rather than considering the actual hydraulically driven flooding, result in imprecise assessments of compound flooding risk. Numerous studies have explored coastal flooding stemming from TCs and ETCs through the utilization of physics-based modeling methodologies (Marsooli et al., 2019; Gori et al., 2020; Emanuel, 2017; Lin et al., 2019). However, the majority of these studies have primarily focused on single hazard scenarios, such as rainfall- or surge-induced flooding, or on combining separate hazards. Therefore, these approaches may underestimate flooding risk when modeling the hydrodynamics of compound flooding. In our study, we employ an innovative approach designed to overcome the limitations often associated with these conventional methodologies. Our method utilizes a physically-based numerical hydrodynamic model, allowing for the explicit simulation of compound flooding. This is accomplished by concurrently converting key driving factors, such as wind speed and rainfall intensity, into hydraulic-based flood simulations, providing a high level of temporal and spatial resolution to comprehensively capture the complex interplay between surge and rainfall-driven flooding during the landfall of TC or ETC storms.

By utilizing a state-of-the-art dataset of downscaled storms, combined with an understanding of the climatology of these storms and projected sea level rise (SLR) in the current and future warming climate, we can evaluate the potential evolution of compound flooding risk in coastal areas. This approach also allows us to identify the primary drivers that may intensify the risk of compound flooding. Such information can furnish a detailed granular perspective on the risk of compound flooding in coastal regions, enabling authorities to enhance their preparedness and adaptation strategies for coastal cities and communities. This proactive approach is crucial for mitigating damages in the current and future climates.

2 Dataset and methodology

Synthetic Tropical Cyclone Model and Datasets

To comprehensively address the multiple hazards associated with TCs, we initiate the process by creating synthetic TC events using the methodology detailed in references (Emanuel et al., 2006, 2008). This method employs deterministic and numerical downscaling to generate synthetic TCs by introducing random seeding, both in terms of their spatial and temporal characteristics, across the entire Atlantic Ocean basin. The initial wind intensity of these seeded TCs is determined through a deterministic calculation, utilizing a high-resolution, coupled ocean-atmosphere tropical cyclone model. This model is driven by the thermodynamic conditions of the ocean and atmosphere, taking into account various factors, including monthly mean sea surface temperature, atmospheric temperature, humidity, and daily interpolated horizontal winds at altitudes of 250 and 850 hPa (Emanuel et al., 2008).

It's important to note that any storms failing to intensify to wind speeds exceeding 21 m/s (equivalent to 40 knots) are excluded from the dataset. In a natural selection process, only seed vortices encountering favorable large-scale environmental conditions intensify into TCs, with their development timing synchronized with environmental climatic patterns. The intensity of TCs is determined through the employment of the Coupled Hurricane Intensity Prediction System (CHIPS), which is an axisymmetric hurricane model coupled to a 1D ocean model (Emanuel et al., 2004). For the purposes of this study, we fix the TC outer radius at 400 km, but otherwise, the structure of the vortex, including the radius of maximum winds, is determined by the model physics. The dynamic downscaling method enables the simulation of numerous synthetic TC events, driven by bias-corrected climate reanalysis or projections from CMIP6 GCMs. Throughout the entire lifespan of each synthetic TC, we consistently record key meteorological parameters, including maximum surface wind speed, pressure, and the radius of maximum winds. These parameters are obtained through the model and are saved at 2-hour intervals. Subsequently, a hydrodynamic model known as GeoClaw (Mandli & Dawson, 2014) is employed to simulate wind-induced storm surges with high temporal resolution along the coastline near the study area during the landfall of each synthetic TC (further details on this modeling process can be found in the provided references).

In addition to generating primary drivers for storm surges from synthetic TCs, we also generate high-resolution hourly rainfall intensity data at a spatial resolution of approximately 20 meters for the vicinity of the study area during the landfall of each synthetic TC using a Tropical Cyclone Rainfall (TCR) model (Feldmann et al., 2019). TCR, a physics-driven model, links convective rainfall in TCs to the TC vortex's vertical velocity, accounting for factors such as frictional convergence, topography, vortex stretching, baroclinic effects, and radiative cooling. Previous studies have applied TCR in risk assessments (Emanuel, 2017; Gori & Lin, 2022) and validated it against observed TC-related rainfall in the United States (Feldmann et al., 2019; Xi et al., 2020). These studies demonstrated TCR's accuracy in replicating coastal rainfall patterns but noted limitations in inland and mountainous areas. To assess the accuracy of this rainfall dataset, Feldmann et al., (2019) conducted an evaluation by comparing it with observed rainfall data obtained from the NEXRAD radar network and rain gauges across the eastern United States. This high-resolution, hourly rainfall intensity data plays a critical role in quantifying the rainfall-induced hazard, a key component contributing to the compound flooding processes.

The downscaling process is implemented for six distinct CMIP6 climate model simulations: CESM2, CNRM-ESM2-1, EC-EARTH3, IPSL-CM6A-LR, MIROC6, and UKESM1-0-LL, all operating under the SSP3-7.0 scenario. Synthetic TC tracks are generated for two different time periods: the late 20th century, spanning 1971-2000, and the end of the century, from 2071-2100, using the climate model simulations. The whole dataset comprises approximately 46,800 synthetic storms, with approximately 3,900 synthetic storms generated from each climate model in each period. Furthermore, we repeat this process to generate 4,100 synthetic storms based on NCEP reanalysis data, representing the late 20th century and current climates (1979-2020). In total, these datasets encompass a large set of synthetic TCs, with their centers passing within 300 km of the New Bedford city in the study area.

Extratropical cyclone datasets

The method described above, which involves statistically and deterministically downscaling TCs, enables the simulation of a vast number of idealized synthetic TC events based on climate reanalysis or climate model simulations (Emanuel et al., 2008). This is possible, to a reasonable extent, because the feedback of TCs on the surrounding large-scale environment does not significantly impact their subsequent evolution. For example, TC tracks are primarily determined by the large-scale flow in which they are embedded (and, to a lesser extent, by the beta drift effect), which passively advects them (Emanuel et al., 2006), irrespective of the TC's internal evolution. Additionally, this method employs analytical simplifications, such as assuming axisymmetry and moist slantwise-neutrality in the free troposphere, which reduces the downscaling model to a single radial dimension, making it computationally efficient, even at high radial resolution.

However, for ETC events, it is not feasible to neglect the effects of the storm on the large-scale environment. Therefore, it is not possible to generate additional synthetic ETCs within a given global climate model run. Only storms explicitly simulated in these runs can be dynamically downscaled. At present, there are no reduced-dimension models that can be used to dynamically downscale ETCs, so computationally expensive regional climate models like the Weather Research and Forecasting (WRF) model (Komurcu et al., 2018) are required to provide high-resolution information on the behavior of ETCs for risk assessment. Due to the difficulty and computational cost associated with simulating a large number of downscaled ETC events, we do not attempt to do this ourselves. Instead, we utilize state-of-the-art WRF dynamical downscaling data described in Komurcu et al., (2018). These downscaling simulations were developed to support regional climate studies in the northeastern U.S. They downscale CMIP5, RCP8.5 projections by CESM v1.0, which have been bias-corrected to support climate research. The WRF data used here covers two different time periods: the 2006-2020 current climate period and the 2081-2100 end-of-the-century period, with hourly time resolution. Additionally, we use the output of a 2006-2015 WRF simulation to downscale ERA-Interim reanalysis data (Dee et al., 2011), which aids in verifying our model. The WRF simulations employ nested domains on a Cartesian grid, with the innermost domain covering 1500 km by 1200 km and using uniform convection-permitting 3 km resolution. To simulate rainwater flooding and storm surge in the study area, we require downscaled precipitation rates, surface pressure, and surface winds, which must be transformed from the WRF Lambert conformal conic projection to the geographical coordinates used in the hydraulic and surge models. More detailed information can be found in Sarhadi et al. (2024).

To assess the risk associated with compound flooding, we compile a catalog of potential freshwater and surge flooding events linked to ETCs for each downscaled period. To identify potential freshwater flooding events, we calculate time series of rainfall intensity averaged over the area extending from -71.2 to -70.5 W and 41.5 to 41.9 N for each historical and future period. Potential freshwater flooding events are selected iteratively by searching for rainfall intensity maxima in the time series in decreasing order, starting from the global maximum. Each event extends from four days before to one day after the selected local maximum. Once an event is defined, its full time-span is removed from the time series so that the next, slightly weaker event selected is the most intense remaining event in the time series. The total number of events selected in each downscaled period is equal to five times the number of years in the corresponding period. Similarly, to identify potential surge flooding events, we select maxima in a time series of the wind component oriented toward the coast averaged over a 2° × 2° box off the coast of the western Buzzards Bay area. It's important to note that the instantaneous precipitation intensity averaged over the study area and the average wind component oriented toward the coast are only rough predictors of freshwater and storm surge flooding. However, the number of selected rainfall and wind events is sufficient to ensure that all events capable of producing significant freshwater or surge flooding are included. To avoid including tropical cyclones, we only seek events occurring between October and May. We acknowledge that there may be some overlap between TCs and ETCs in October.

Storm surge modeling

Consistent with previous research (Reed et al., 2015; Lin et al., 2016; Garner et al., 2017), we define a storm surge as the anomalous elevation of sea level above Relative Sea Level (RSL). This elevation results from the low atmospheric surface pressure and the high surface wind speed associated with TCs or ETCs. The combination of storm surge and RSL fluctuations characterizes the surge height in coastal regions caused by TCs and ETCs. Our RSL estimation is based on the local average of the total sea level throughout each climate period. RSL also serves as the key factor for distinguishing between land and water elevations. As a result, we disregard interannual sea level variations and the relatively minor nonlinear interactions between the surge and RSL, as outlined in prior studies (Lin et al., 2016). Furthermore, astronomical tides are not factored into our calculations. It is important to note that future studies should investigate the effects of tides and their nonlinear interactions with surges, particularly in light of potential changes due to SLR (Müller, 2011; Garner et al., 2017).

To simulate storm surges generated by synthetic TCs and ETCs, we utilize the GeoClaw numerical model, which relies on high-resolution shock-capturing finite volume methods (Mandli & Dawson, 2014). Unlike finite-element unstructured hydrodynamic models (Colle et al., 2008; Westerink et al., 2008), GeoClaw incorporates Adaptive Mesh Refinement (AMR) algorithms (Berger et al., 2011; Mandli & Dawson, 2014), enabling efficient computational solutions at high resolutions over large scales. We implement a broad domain, covering approximately 1000 kilometers, to better quantify the large-scale impact of various attributes of TCs and ETCs, including intensity, duration, size, and landfall location, on storm surges. Along the coastline in the study area, we position synthetic gauges to provide comprehensive coverage. These gauges record surge heights at high temporal resolutions, typically less than a minute, during each individual landfall of TCs and ETCs. We also employ an interpolation method to derive surge heights at additional synthetic gauges distributed along the entire coastline. Consequently, these coastal surge conditions are transformed into surge-driven flooding through a hydraulic model, allowing us to model the propagation of surges and their potential to cause surge-driven flooding in coastal areas. This surge simulation approach is applied to a broad set of synthetic TC and ETC events. It's worth noting that the performance of GeoClaw in modeling TC surges has been evaluated in previous studies (Miura et al., 2021; Mandli & Dawson, 2014; Sarhadi et al., 2024). Through the incorporation of critical enhancements, we have expanded GeoClaw's functionality to effectively model storm surges resulting from ETCs, thereby surpassing the default settings of the out-of-the-box model.

Figure 1 illustrates the surge modeling process, which entails dynamically downscaled WRF simulations of primary surge drivers, including wind and pressure fields, forced by ERA-Interim reanalysis data. The simulation corresponds to a historical ETC event that occurred on December 27-28, 2012, within the study area. The model's performance accuracy is depicted in Figure 1. The simulated surge, using the modified GeoClaw model, demonstrates a robust agreement with observed surge levels. These observed surge values were obtained by de-tiding water levels, a procedure that involves subtracting water elevation from NOAA tide predictions at the Woods Hole gauge.

For modeling surges generated by TCs and ETCs during the late 20th century and in the current climate, we rely on RSL data obtained from NOAA gauge observations. However, in the context of future climate scenarios, we incorporate SLR projections derived from CMIP6 under the SSP3-7.0 scenario into GeoClaw using a bathtub approach. This allows us to quantify the impact of SLR on the changing risk of surges and compound flooding. The methodology involves calculating the ensemble mean of total SLR over future climate scenarios (Fox-Kemper et al., 2021). These projections encompass comprehensive considerations, including the contributions of Antarctic and Greenland ice sheets, glacier dynamics, thermal expansion of seawater, terrestrial water storage, vertical land motion, and the potential influences of marine ice cliff instability.

Numerical compound flood modeling

To simulate the intricate hydrodynamic interactions involved in compound flooding, a confluence of storm surges and heavy inland rainfall stemming from synthetic TCs and ETC events, we modified a version of the LISFLOOD-FP model. This two-dimensional hydraulic model, renowned for its high spatio-temporal resolution, is recognized for its computational efficiency. A detailed description of this model is provided in reference (Neal et al., 2012). LISFLOOD-FP employs an explicit finite difference scheme to simulate shallow water waves, while deliberately omitting advection (Bates et al., 2010). The efficacy of the fundamental model's numerical scheme in simulating pluvial and fluvial flood dynamics has been substantiated by various studies (Neal et al., 2012; Wing et al., 2022; Bates et al., 2021). In our work, this model has been customized to incorporate high-resolution surge height data (simulated by GeoClaw) along the coastline, and simultaneously, it accommodates hourly rainfall intensity data from storm events in the inland regions as boundary conditions. This physically based approach empowers the model to replicate the dynamics of compound flooding in response to the rapid spatio-temporal fluctuations in surge and rainfall driven flooding during the landfall of each storm. The model ensures the conservation of mass within each grid cell and maintains the continuity of momentum of compound flooding between neighboring cells. The model recalculates the flow depth, taking into account the elevation of each cell, water surface slope, surface Manning's roughness coefficient, and acceleration due to gravity. More details about the methodology can be found in Sarhadi et al. (2024).

It's important to note that the geodetic datum of NAD83 is utilized to establish the spatial coordinates, while the vertical datum of NAVD88 is used for elevation values within the applied Digital Elevation Model (DEM). In our study, we utilize a LiDAR-based DEM with an approximate spatial resolution of 20 m, employing a geographic (Lat/Lon) projection to represent the area's geometry. A land-use map is employed to quantify surface roughness, and a map of available soil water storage for the topsoil layer (0-50 cm) is used to account for the infiltration rate in non-constructed areas. The source of these input files is given in the data availability section.

In this process, the hydrodynamics of compound flooding during the landfall of each storm are comprehensively simulated with high temporal and spatial resolution. We then store the maximum compound flooding level at each grid cell for every individual storm event. This process is iteratively conducted for a vast set of TCs and ETCs derived from reanalysis and climate models. These maximum flood records serve as a reflection of the compound flooding behavior over each defined time period for every grid cell. Subsequently, these records are fundamental in constructing a nonparametric empirical Cumulative Distribution Function (eCDF). This approach leverages the theory of nonexceedance probability to determine the return period of a compound flooding event at each grid cell.

The calculation is expressed as:

$$T_H(h) = \frac{1}{P(H > h)} \tag{1}$$

In this equation, $P(H > h)$ signifies the annual probability that the compound flooding level of an event (H) exceeds a specific threshold (h), and $T_H(h)$ corresponds to the return period of that particular event. The ensemble mean of compound flooding levels for TCs and ETCs at various return periods is then computed by considering multiple climate models across distinct time periods. The assessment of expected changes in compound flooding levels at specific return periods is carried out by evaluating the disparities between the ensemble mean of flood levels in future climate scenarios and those in past or current climate conditions. To dissect the individual and collective influences of changes in storm climatology and SLR on the granular risk of compound flooding, our approach involves running the hydraulic model twice for each individual storm. This includes one simulation with the incorporation of SLR and another without it. This approach allows us to discern and quantify the distinct and synergistic effects of variations in storm climatology and SLR on the risk of compound flooding. To distinguish the contribution of each individual hazard (surge or rainfall-driven flooding) in compound flooding from each storm, we can simply run the model with only one driver as the boundary condition.

3 Results and Discussion

Impact of primary driver severity on compound flooding

Here, we evaluate the influence of the primary drivers during the landfall of TCs on the magnitude and extent of inundation associated with compound flooding in the study area. This assessment is pivotal for gaining a comprehensive understanding of the intricacies inherent in flood hazards stemming from these meteorological phenomena. High wind speeds and low atmospheric pressure during the landfall of TCs lead to storm surge-driven flooding along coastal regions. Specifically, the greater the wind speed, the more intense and higher the storm surge becomes both before and during landfall. Concurrently, rainfall intensity during landfall contributes to rainfall-driven flooding. The interplay between these factors, as elucidated in this study, sheds light on the intricate mechanisms that underpin the devastating consequences of compound flooding induced by TCs. The severity and dominance of each primary driver determine the corresponding severity of the compound flooding hazard. Depending on which primary driver predominates, it may result in scenarios such as compound flooding with a dominant surge in coastal areas, a situation where rainfall-driven flooding in inland areas is more pronounced, or instances when both drivers are strong, leading to a severe compound flooding event characterized by both surge and rainfall-driven inundation.

By examining the magnitude of these primary drivers, our study offers essential insights into the dynamics of compound flooding, encompassing factors like magnitude and the extent of inundation. To illustrate this, we selected two TCs as case studies to demonstrate how the magnitude of primary drivers can affect the resulting compound flooding. Figure 2 (top panels) presents information on the primary drivers of these two synthetic TC storms, which were derived from downscaling NCEP reanalysis data for the current climate. These measurements are presented both prior to landfall and at the time of landfall.

In the first case, represented by synthetic track #1337 (Fig. 2, A and B), the primary drivers include strong wind speeds (knots) at the eye of the TC before and during landfall, with rainfall intensity reaching up to 90-120 mm/hr in certain grid cells and an average wind speed of 40 knots (though it's important to consider the duration of high wind speeds too). These primary drivers result in flooding depths of up to 3 meters in some low-land coastal and inland areas. In contrast, the second case, depicted by synthetic track #1339 (Fig. 2, C and D), exhibits lower rainfall intensity, with the upper tail reaching up to 10 mm/hr, and wind speeds at the eye barely reaching 40 knots in the upper tail. These conditions lead to significantly lower flooding, especially in inland areas, and a reduced presence of compound flooding in coastal areas, where the flooding is predominantly surge-driven.

This understanding offers a comprehensive and scientifically robust exploration of the relationship between the magnitude of primary drivers—specifically, rainfall intensity and surface wind speed—and the resulting complex dynamics of compound flooding. These insights are invaluable for advancing our understanding of the multifaceted flood hazards associated with TCs, which, in turn, contribute to a more informed and resilient approach to disaster preparedness. Using this approach, one can easily quantify the proportion of each individual hazard and analyze the dynamic interplay between them in generating compound flooding, with high temporal and spatial resolution. Notably, the same methodology can be readily applied to ETC storms. This deeper understanding supports improved forecasting, risk assessment, and preparedness measures in vulnerable coastal regions, ultimately enhancing resilience against the impacts of these storms. In the subsequent section, we delve into the contribution of each individual and compound hazard to the risk assessment and emphasize the significance of a physics-based approach to compound flooding.

Assessing compound flooding impact and risk

In this section, we present a comparative analysis of compound flooding, delineating the individual contributions of surge and rainfall-driven flooding with a focus on coastal areas. The objective is to offer a clearer understanding of the effects and potential risks associated with compound flooding. Additionally, we examine how other approaches, such as singular hazards, surge, and rainfall-driven flooding considered individually, or a linearly additive hazards approach, may lead to the underestimation or overestimation of the risk. It is important to note that our comparisons are based on the results obtained from six climate models. This approach enhances clarity by visualizing differences in various sources of flooding within the models and accounting for uncertainties among them.

To better comprehend the impact and importance of compound flooding in risk assessment for both the late 20th and 21st century climates, we selected a specific coastal area, which is also an urban area, as depicted in Figure 3 (A). This area was chosen to predominantly consist of non-tidal ground areas, with intertidal zones excluded, facilitating a comparative risk analysis. We evaluated the risk, defined by probability of occurrence or return period, associated with single hazards: surge-driven flooding (represented in green), rainfall-driven flooding (in blue), and compound flooding, which takes into account the complex hydrodynamic interplay between these hazards at high temporal and spatial resolutions (depicted in red). We also included a linear addition of individual flooding as a commonly used approach (in brown). This comparative analysis is instrumental in discerning the biases that arise when individual hazards are considered separately or when the two are merely linearly combined to assess flooding risk, without accounting for the intricate hydrodynamic interactions across time and space inherent in compound flooding.

As depicted in Figure 3, during the late 20th century, a significant proportion of compound flooding contributions originated from rainfall-driven flooding rather than surge-driven flooding, for both high-frequency and low-frequency events in nearly all climate models. This emphasizes the risk underestimation resulting from relying solely on surge-driven flooding in this region. Conversely, the linear summation of the two individual hazards, without accounting for the complex hydrodynamics of their interaction during landfall, results in an overestimation of risk in the majority of the climate models.

Moving forward to assess the risk at the end of the 21st century, a significant increase is observed in both individual and compound flooding risks, driven by alterations in storm climatology and SLR. Although, compared to the 20th century, the risks of both rainfall-driven flooding and surge-driven flooding increase significantly; however, unlike the end of the 20th century, surge-driven flooding dominates and contributes more to compound flooding compared to rainfall-driven flooding in this area, especially for low-frequency events (with return periods above 50 years). For specific upper tail low-frequency events, there is a heightened prominence of surge-driven flooding, contributing to compound flooding (in almost all climate models except UKESM1-0-LL), compared to rainfall-driven flooding. Additionally, the risk of compound flooding intensifies; events that previously occurred once every 100 years in the late 20th century will pose a risk of occurring almost every less than 5 years by the end of the 21st century in almost all climate models. It is also worth noting that simply linearly summing the two single hazards together to assess compound flooding results in a significant overestimation of the risk in the future climate. For example, events that occur approximately every 500 years (factoring in the complex hydrodynamic interplay between surge and rainfall-driven flooding) are estimated to happen approximately every 75 years by the end of the century when individual hazards are simply added linearly, signifying a considerable bias and overestimation in risk assessment.

The results initially emphasize the significance of employing a physics-based model for downscaling TCs under the context of a future warming climate. This approach is crucial for an accurate assessment of risk, as it takes into account the influence of climate change in the forthcoming decades. This stands in contrast to relying solely on historical records, which do not accurately represent the characteristics of storms in the future warming climate and overlook the profound impacts of climate change on TC behavior. The results also underscore the importance of considering the explicit complex hydrodynamics interplay between the individual flooding hazards when assessing the risk, as neglecting it was the case in previous studies (Reed et al., 2015; Lin et al., 2016; Garner et al., 2017; Emanuel, 2017; Marsooli et al., 2019; Lin et al., 2012), can lead to a severe underestimation of the actual risk in both current and future climates, with the discrepancy becoming more pronounced due to changes in climatology and SLR.

Sea level rise and tropical cyclone climatology impacts

SLR and changes in TC climatology are recognized as the primary drivers behind alterations in the risk of compound flooding in coastal regions. SLR, largely attributed to global climate change, raises the baseline water level, rendering coastal areas more susceptible to inundation. When coupled with anticipated shifts in storm climatology, including variations in cyclone tracks, intensification, frequency, and other relevant attributes, the potential for compound flooding becomes increasingly evident. In this section, we investigate the compounding effects of SLR and changes in storm climatology, analyzing their influence on the risk of compound flooding during the late 20th century and the late 21st century. The late 20th century serves as a baseline for comprehending historical trends, while the late 21st-century projection offers insights into future warming scenarios.

Figure 4 shows the compound flooding level from a large set of synthetic tracks in the previously selected coastal area (depicted in Figure 3 (A)), both with and without SLR in the late 20th and 21st centuries, based on the output from six climate models. This analysis aims to better understand the effect of SLR on changing the risk of compound flooding and associated uncertainty within and among different climate models. In the late 20th century, as depicted in Figure 4, SLR does not exhibit a discernible effect on the risk of compound flooding caused by TCs. During this baseline period, the risk of experiencing compound flooding with a 0.5-meter depth, for example, is approximately 1% per annum on average, based on the ensemble of the six climate models, both with and without SLR. As we progress towards the end of the century, changes in storm climatology, without considering the SLR effect, are projected to elevate the risk of compound flooding events. This elevation is manifested with a 10% probability per annum based on the CNRM-ESM2-1 model (Figure 4-D). This projection indicates that changes in storm climatology alone will escalate the risk of 0.5-meter events tenfold compared to the late 20th century. However, when we consider the added contribution of SLR by the end of the century, the risk of a compound flooding event of this nature will increase significantly. It is projected to occur approximately with a 20% probability per annum. This signifies that the combined impact of SLR and changes in storm climatology will amplify the risk twentyfold compared to the late 20th century. Furthermore, SLR alone will elevate the occurrence of such compound flooding events tenfold compared to the late 20th century and increase the annual probability of such an event to 10%. Similar intensification patterns are observed in other climate models. The intensification resulting from the combined impact of SLR and changes in storm climatology significantly amplifies the risk of low-frequency events in the late 21st century. For instance, events that historically had a return period of 1000 years in the late 20th century are projected to occur 40 times more frequently by the end of the century in the majority of the models. In terms of the depth of compound flooding events with a return period of 1000 years in the selected coastal area, the EC-EARTH3 model estimates it to be approximately 0.75 meters (ranging from 0.6 to 0.8 meters) in the late 20th century. However, by the end of the century, the depth of events with the same return period is projected to be around 1.65 meters (ranging from 1.5 to 1.8 meters) due to the combined effects of SLR and changes in storm climatology.

Another noteworthy observation is that SLR is expected to significantly increase the risk of low-frequency events in the upper tail compared to other medium or high-frequency events by the end of the century. In a warming climate, all climate models (except EC-EARTH3 and UKESM1-0-LL) show that SLR is projected to intensify the risk significantly for upper tail events. For example, an extreme event that might occur almost once every 2000 years (based on the CNRM-ESM2-1 model) by the end of the century would have a depth of compound flooding without the impact of SLR at almost 2.4 meters. However, with SLR's impact by that time, the depth is projected to increase to around 3.3 meters in such a warming climate. This difference is smaller in medium to high-frequency events.

Our methodology enables us to examine and elucidate how these interacting primary drivers may influence the risk of compound flooding in a warming climate, providing valuable insights into the adaptive strategies and mitigation measures required for the late 21st century to safeguard coastal communities and infrastructure in an evolving climate. These analyses furnish detailed granular information about which primary drivers are of greater concern and how adaptive strategies can be tailored for each specific area based on priorities.

Tropical cyclone compound flooding risk in today's climate

Here, we utilize our methodology to quantitatively assess the impact of anthropogenic warming that has already occured on the risk of compound flooding, specifically through TC climatology and SLR, within the context of the current climate in the study area. To achieve this, we conduct simulations to determine the maximum compound flooding levels from 4,100 synthetic TCs. These TCs are downscaled from NCEP reanalysis data for two distinct climate periods: the late 20th century (1979-1999) and the early 21st century (2000-2020). Figure 5 (A) illustrates alterations in the level of compound flooding events for different return periods between these two time frames, focusing on a selected location close to the shore, encompassed by buildings and road networks.

Our results suggest no significant changes in the risk of high-frequency events (less than 50 years) in the current climate compared to the late 20th century. Furthermore, they suggest a slight increase in the magnitude of compound flooding, characterized by return periods exceeding 50 years, under today's climate compared to the late 20th century. This intensification is observed for rare events as well. However, it is important to note that distinguishing distinct trends for these events proves challenging due to sampling uncertainties.

In Figure 5 (B), we present the spatially distributed risk of compound flooding events occurring once every 100 years or with a 1% likelihood of occurring in any given year across the entire study area. The outcomes suggest that climate change has notably elevated the flood levels associated with such events, particularly in low-land coastal and inland areas, resulting in an increase of up to 0.4 meters, though the sampling uncertainty is large at these return periods. Notably, there is no observed decrease in the level of flooding within the region. These results underscore the profound influence of climate change on TC characteristics, including wind speeds, in conjunction with SLR, intensified rainfall, and the consequential surge height and compound flooding along coastlines, as well as inland flooding. Our findings underscore the pivotal role of climate change in reshaping the risk of compound flooding in the study area. A nuanced understanding of this evolving risk provides valuable insights for decision-makers, even in the short term, within the current climate as compared to the past. This knowledge aids in identifying areas that are most vulnerable to these hazards, thereby facilitating more informed decision-making processes in the current climate.

Tropical cyclone compound flooding risk in a future warming climate

Here, we conduct a comprehensive analysis of compound flooding risk associated with TCs, focusing on how this risk may evolve in a warming climate. Our investigation considers changes in TC climatology and SLR across different time periods. To understand the temporal evolution of compound flooding risk in our study area, we center our analysis on a specific location near New Bedford City, as indicated in Figure 6. Our aim is to illuminate the changing dynamics of compound flooding depths in this area, drawing insights from historical data, contemporary observations, and future climate projections.

We conducted a rigorous probabilistic analysis, employing advanced mixture modeling techniques to delineate the underlying probability distributions of compound flooding for each time period. Specifically, gamma and Weibull mixture models were applied to simulated compound flooding levels from each climate model, with model selection guided by the Akaike Information Criterion (AIC). To comprehensively assess inherent uncertainty, we applied bootstrap resampling techniques, generating 3,000 samples per iteration for compound flooding level simulations from each climate model across each time period. Subsequently, confidence intervals at the 5% and 95% levels were derived for key parameters associated with the fitted distribution. The frequency of compound flooding in the specified regions, attributed to changes in storm climatology and SLR, is delineated in Figure 6 through aggregated simulations involving six CMIP6 climate models. In this figure, the bold line represents the frequency of compound flooding levels within the selected area for different return periods across distinct time periods, including simulations for the late 20th and 21st centuries, as well as reanalysis data from the NCEP dataset for the current climate. Furthermore, the colored envelope illustrates the ensemble mean within the 5th to 95th percentile range, calculated based on the outcomes derived from the six climate models. The results (based on the ensemble mean of the climate models) indicate that compound flooding events that previously occurred with a 1% probability in a given year, in the late 20th century in this particular location, have now increased in frequency. In the current climate, these events occur with an annual probability of 1.3 in any given year, and in the future, they are expected to occur with a probability of 3.3 in each year. Evidently, changes in storm climatology and SLR are leading to a significant increase in the risk of compound flooding in the selected area. Furthermore, in a future warming climate, the depth of compound flooding associated with low-frequency events from TCs will also substantially increase. For instance, for events with an annual probability of 0.2%, the depth of compound flooding in this specific area is projected to rise from approximately 0.5 meters in the current climate to 1.25 meters by the end of 21st century. Therefore, it is crucial that the design of infrastructure, housing, and other critical facilities takes into account the heightened risk of compound flooding from TCs, both in the present and in the face of future, intensifying storms and SLR.

To gain a comprehensive understanding of the spatially distributed risk of compound flooding in the area, we have calculated the risk for each grid cell with a 20-meter spatial resolution, drawing from the extensive simulations of synthetic TCs. Figure 7 illustrates the results for different types of compound flooding events with return periods of 5, 50, 200, and 500 years. This spatial analysis provides valuable insights into the risk associated with both high-frequency and low-frequency compound flooding events from TCs. For each time period, including the late 20th century (Figure 7 A-D) and the 21st century (Figure 7 E-H), we assessed the depth of compound flooding for various high and low-frequency events at the grid cell level. To understand the role of changes in storm climatology and SLR in reshaping the risk landscape of compound flooding in warming climate in the study area, we have used the late 20th century as a baseline for comparison. The ensemble mean of compound flooding for each return period was analyzed to discern trends and shifts in the occurrence and intensity of compound flooding from TCs. Figure 7 (I-L) reveals that, for high-frequency events, the level of compound flooding resulting from intensified TCs and SLR will increase by 0.5-1.0 meters in coastal areas and by 2.0-2.5 meters for low-frequency events in the same regions. In inland areas, the risk of flooding from intensified rainfall associated with TCs in a warming climate will increase significantly, with flooding levels rising by 1.5-2.5 meters for low-frequency intensified TCs in the majority of areas.

The detailed, granular information provided in this section regarding compound flooding in the late 20th century and in a warming climate in the late 21st century is crucial for tailoring effective adaptation strategies in infrastructure design, as well as for the construction of buildings and critical infrastructure such as power plants. This information is also important for formulating policies and structuring insurance to discourage habitation in high-risk locations. Relying solely on historical risk assessments, even when extensive information is available, as depicted in Figure 7 (A-D), is insufficient. This is because the risk of compound flooding driven by TCs in future warming decades will surpass historical risk due to changes in storm climatology and SLR (Figure 7 (E-H)). Our physics-based risk assessment methodology provides a comprehensive understanding of the compound flooding risk linked to TCs, spanning historical, current, and future scenarios. Through the comparative analysis of return periods across different temporal frames, our findings serve to inform and direct strategies for mitigating and adapting to the complex challenges presented by compound flooding in a continually evolving climate. Therefore, it is desirable to ground design decisions in physics-based risk assessment outcomes tailored to the future warming climate to establish resilience in infrastructure, urban development, and community preparedness.

Extratropical cyclones compound flooding risk in current and future climates

In Figure 8, we illustrate the contributions of ETC climatology changes and SLR to variations in the risk of compound flooding within the depicted area, encompassing both current and anticipated future warming climates. Our analysis is limited to high-frequency events, defined by return periods of 20 years or less, due to constraints associated with our downscaled dataset. The combined impact of ETC climatology changes and SLR is projected to lead to a nearly threefold increase in the likelihood of compound flooding by the end of the century in the selected coastal area. Specifically, compound flooding events with high-frequency occurrences, with a 5% annual probability, are expected to occur with a 14% annual likelihood by the end of the century. These pronounced changes are primarily observed in the coastal areas.

To gain deeper insights into the effects of ETC climatology change and SLR, we also quantify the spatially varying risk of compound flooding events in the current and future warming climate. Figures 9 (A-D) depict the results for the current climate, while Figures 9 (E-H) display the projections for the end of the century. In Figures 9 (I-L), we highlight differences in flooding levels across different regions for the specified return periods. Evidently, coastal areas exhibit a pronounced intensification of compound flooding, attributed primarily to SLR within these regions. The magnitude of this intensification in compound flooding levels increases from events with return periods of 2 years to those with return periods of 20 years. However, unlike TC-driven compound flooding, the levels of flooding resulting from ETC events in inland areas display a distinct pattern for high-frequency ETC events. Our findings indicate no discernible trend in terms of flooding levels in inland areas at the end of the 21st century, relative to the current climate. In fact, some areas even exhibit a decreasing trend, with only some low-lying regions displaying an increasing trend, which is not statistically significant when compared to the current climate. Therefore, our results suggest that rainfall-driven flooding from high-frequency ETC events will not intensify in inland areas from future ETC events relative to the ones in the current climate. The bulk of the intensification is expected to occur along coastal areas, driven primarily by SLR during high-frequency ETC events. These findings align with prior studies (Lin et al., 2019; Booth et al., 2021), which indicate that the effects of climate change on ETC storms are relatively minor compared to the significant impact of SLR on storm surge intensification in northeastern U.S. coastal areas. To enhance our understanding and facilitate comparisons, it is imperative to include more dynamically downscaled ETC events over longer time periods, particularly focusing on low-frequency events. This would allow us to comprehensively assess the risk of compound flooding associated with these low-frequency ETC events, similar to the approach taken in our analysis of TC-driven compound flooding events.

4 Conclusion

In this study, we employed a physics-based risk assessment methodology designed to quantify the risk of compound flooding stemming from tropical and extratropical cyclones in coastal regions. We emphasize the virtues of a physics-based approach, which circumvents the severe limitations of historically based assessments, given the shortness of the records and the growing irrelevance of history in a changing climate. Such methods are essential for understanding the evolving landscape of compound flooding risk in coastal areas within the current and future climates. Our methodology offers a comprehensive means of assessing past, present, and future risks under the influence of changing storm drivers and SLR, which amplifies coastal flooding.

To achieve our objectives, we employed a two-pronged approach. First, we downscaled from reanalyses and climate models comprehensive datasets of synthetic TCs using a statistical-deterministic method. Additionally, we downscaled ETCs using WRF. These simulations were informed by key climate statistics and reanalysis data, addressing the challenges associated with the scarcity of relevant datasets over varying time periods. Furthermore, this approach allowed us to account for the influence of climate change on the primary drivers of compound flooding. In order to quantify the risk of compound flooding, our methodology explicitly considers the intricate hydrodynamics of this phenomenon. It takes into account the simultaneous interplay of surge-driven and rainfall-driven flooding across time and space during the landfall of each storm. This unique approach enables us to assess the contribution and magnitude of primary drivers, such as rainfall intensity, wind speed, and SLR, in amplifying compound flooding and backwater effects across both time and space at high resolution. It also facilitates the assessment of the contribution of each individual flooding type to the overall compound flooding risk assessment. Our results underscore the underestimation of both individual flooding hazards and the overall risk of compound flooding stemming from both TCs and ETCs, particularly in a warming climate. This underscores the significance of using numerical simulations that incorporate the complex hydrodynamics of explicit compound flooding caused by TCs and ETCs. This approach emphasizes the importance of moving away from reliance solely on statistical joint distribution of the drivers of compound flooding or conventional statistical or physical methods that focus exclusively on individual drivers or hazards (Gori et al., 2022; Moftakhari et al., 2017; Lin et al., 2019, 2016; Garner et al., 2017; Reed et al., 2015).

Our methodology is instrumental for understanding the contribution of storm climatology changes and SLR to the evolution of compound flooding risk over time. We find that TC-driven compound flooding risk is considerably higher than that of ETC-driven events, especially for high-frequency events in the Buzzards Bay area. Our results further demonstrate an increased risk of TC-driven compound flooding in the present climate compared to the late 20th century, with significant intensification anticipated in future warming climates. SLR emerges as a substantial contributor to this heightened risk. In the case of high-frequency ETC-driven compound flooding, we anticipate an amplified risk in coastal areas by the end of the century, primarily due to SLR. Nevertheless, the risk in inland areas seems to remain relatively stable, with specific regions even experiencing a reduced risk of rainfall-driven flooding.

While our methodology excels at assessing risk associated with rare events, its capacity to evaluate ETC-driven risk is limited by the scarcity of events feasible for simulation using three-dimensional models like WRF. Future research should focus on more efficient methods for downscaling ETC storms, potentially through high-resolution global model ensembles in present and future climates. Though our study did not address the interaction of astronomical tides with storm surge and SLR, we acknowledge their importance and recommend their inclusion in future assessments of surge and compound flood hazards. Our methodology can be extended beyond the Buzzards Bay area and New York City (Sarhadi et al., 2024) and can be applied as a scalable framework for vulnerable coastal regions worldwide that face the imminent threat of compound flooding from TCs and ETCs, even in the absence of historical records, regardless of their latitude. However, it is essential to tailor the methodology to incorporate region-specific factors, such as bathymetry, soil characteristics, coastal morphology, storm surge dynamics, and tidal influences. Customization helps ensure the accurate assessment and quantification of the compound flooding hazard by tailoring the approach to the specific characteristics and conditions of the region or scenario.

Our methodology also equips decision-makers with scientifically-informed insights to enhance preparedness and resilience of coastal areas. It enables authorities to estimate the likelihood of destructive storms in both current and future decades and quantify potential damages. Regional assessments empower authorities to customize adaptation strategies, allocate resources effectively, and safeguard critical infrastructure and coastal communities. Our study can serve as a cornerstone for proactive risk assessment, especially given the projected population increase within flood-prone coastal zones and megacities by 2050 (Aerts et al., 2014; Neumann et al., 2015; Kulp & Strauss, 2019). Notably, despite the significant assets in coastal flood-prone areas, investments in protective measures often fall short. Our methodology provides a comprehensive guide to ensure that adaptation efforts are precisely tailored to address the unique challenges posed by compound flooding in coastal cities. In addition to localized adaptation measures, the need to reduce greenhouse gas emissions takes center stage in mitigating the increased risk and reducing associated damages within a warming climate.

In summary, our research significantly advances our comprehension of the multi-faceted risks associated with compound flooding, while concurrently providing decision-makers with a robust analytical framework and requisite resources to fortify the resilience of vulnerable coastal regions in response to the escalating influence of climate change. Consequently, our study can serve as an essential foundation for the development and implementation of comprehensive strategies encompassing damage mitigation, strategic design, anticipatory planning, predictive forecasting, adaptive measures, and proactive mitigation interventions, all specifically tailored to address the complexities of coastal flooding caused by cyclonic storms.

Acknowledgments

The authors express their gratitude to Muge Komurcu, Matthew Huber, and Stanley Glidden for providing WRF dynamical downscaling data for ETC events. We also acknowledge the World Climate Research Programme, which, through its Working Group on Coupled Modelling, coordinated and promoted CMIP. We thank the climate modeling groups, including CESM2, CNRM-ESM2-1, EC-EARTH3, IPSL-CM6A-LR, MIROC6, and UKESM1-0-LL for producing and making available their model output. Financial support for this work was provided by Homesite Insurance.

Data availability statement

For surge modeling, historical SLR data in the study area were obtained from NOAA (`https://www.tidesandcurrents.noaa.gov/sltrends/`). The CMIP6 SLR projections under the SSP3-7.0 scenario are also available at `https://sealevel.nasa.gov/ipcc-ar6-sea-level-projection-tool?psmsl\_id=12`. Additional data utilized in flood modeling, such as current bathymetry and coastal features, can be obtained from the following source, `https://www.ncei.noaa.gov/maps/bathymetry/`. The LiDAR-based Digital Elevation Model (DEM) with a computationally feasible spatial resolution of ~ 20 m to represent the topography of the area is available at `https://coast.noaa.gov/dataviewer/`. The landuse map to quantify surface roughness is accessible at `https://www.mrlc.gov/`. A map showing soil available water storage, which is used to assess top-soil infiltration rates, can be found at `https://websoilsurvey.sc.egov.usda.gov/`. Synthetic TC tracks are based on the methodology described by Emanuel et al. (2006), and ETC event data are available from Komurcu et al. (2018).

References

Aerts, J. C., Botzen, W. W., Emanuel, K., Lin, N., De Moel, H., & Michel-Kerjan, E. O. (2014). Evaluating flood resilience strategies for coastal megacities. *Science*, *344*(6183), 473–475.

Bakkensen, L. A., & Mendelsohn, R. O. (2019). Global tropical cyclone damages and fatalities under climate change: An updated assessment. *Hurricane risk*, 179–197.

Bates, P. D., Horritt, M. S., & Fewtrell, T. J. (2010). A simple inertial formulation of the shallow water equations for efficient two-dimensional flood inundation modelling. *Journal of Hydrology*, *387*(1-2), 33–45.

Bates, P. D., Quinn, N., Sampson, C., Smith, A., Wing, O., Sosa, J., … others (2021). Combined modeling of us fluvial, pluvial, and coastal flood hazard under current and future climates. *Water Resources Research*, *57*(2), e2020WR028673.

Berger, M. J., George, D. L., LeVeque, R. J., & Mandli, K. T. (2011). The geoclaw software for depth-averaged flows with adaptive refinement. *Advances in Water Resources*, *34*(9), 1195–1206.

Booth, J. F., Narinesingh, V., Towey, K. L., & Jeyaratnam, J. (2021). Storm surge, blocking, and cyclones: A compound hazards analysis for the northeast united states. *Journal of Applied Meteorology and Climatology*, *60*(11), 1531–1544.

Colle, B. A., Booth, J. F., & Chang, E. K. (2015). A review of historical and future changes of extratropical cyclones and associated impacts along the us east coast. *Current Climate Change Reports*, *1*, 125–143.

Colle, B. A., Buonaiuto, F., Bowman, M. J., Wilson, R. E., Flood, R., Hunter, R., ... Hill, D. (2008). New york city's vulnerability to coastal flooding: Storm surge modeling of past cyclones. *Bulletin of the American Meteorological Society*, *89*(6), 829–842.

Dee, D. P., Uppala, S. M., Simmons, A. J., Berrisford, P., Poli, P., Kobayashi, S., ... others (2011). The era-interim reanalysis: Configuration and performance of the data assimilation system. *Quarterly Journal of the royal meteorological society*, *137*(656), 553–597.

Emanuel, K. (2017). Assessing the present and future probability of hurricane harvey's rainfall. *Proceedings of the National Academy of Sciences*, *114*(48), 12681–12684.

Emanuel, K., DesAutels, C., Holloway, C., & Korty, R. (2004). Environmental control of tropical cyclone intensity. *Journal of the atmospheric sciences*, *61*(7), 843–858.

Emanuel, K., Ravela, S., Vivant, E., & Risi, C. (2006). A statistical deterministic approach to hurricane risk assessment. *Bulletin of the American Meteorological Society*, *87*(3), 299–314.

Emanuel, K., Sundararajan, R., & Williams, J. (2008). Hurricanes and global warming: Results from downscaling ipcc ar4 simulations. *Bulletin of the American Meteorological Society*, *89*(3), 347–368.

Feldmann, M., Emanuel, K., Zhu, L., & Lohmann, U. (2019). Estimation of atlantic tropical cyclone rainfall frequency in the united states. *Journal of Applied Meteorology and Climatology*, *58*(8), 1853–1866.

Fox-Kemper, B., Hewitt, H., Xiao, C., Aalgeirsdóttir, G., Drijfhout, S., Edwards, T., ... others (2021). Ocean, cryosphere and sea level change.

Garner, A. J., Mann, M. E., Emanuel, K. A., Kopp, R. E., Lin, N., Alley, R. B., ... Pollard, D. (2017). Impact of climate change on new york city's coastal flood hazard: Increasing flood heights from the preindustrial to 2300 ce. *Proceedings of the National Academy of Sciences*, *114*(45), 11861–11866.

Gori, A., & Lin, N. (2022). Projecting compound flood hazard under climate change with physical models and joint probability methods. *Earth's Future*, *10*(12), e2022EF003097.

Gori, A., Lin, N., & Smith, J. (2020). Assessing compound flooding from landfalling tropical cyclones on the north carolina coast. *Water Resources Research*, *56*(4), e2019WR026788.

Gori, A., Lin, N., Xi, D., & Emanuel, K. (2022). Tropical cyclone climatology change greatly exacerbates us extreme rainfall–surge hazard. *Nature Climate Change*, *12*(2), 171–178.

Komurcu, M., Emanuel, K., Huber, M., & Acosta, R. (2018). High-resolution climate projections for the northeastern united states using dynamical downscaling at convection-permitting scales. *Earth and Space Science*, *5*(11), 801–826.

Kossin, J. P. (2018). A global slowdown of tropical-cyclone translation speed. *Nature*, *558*(7708), 104–107.

Kossin, J. P., Emanuel, K. A., & Vecchi, G. A. (2014). The poleward migration of the location of tropical cyclone maximum intensity. *Nature*, *509*(7500), 349–352.

Kulp, S. A., & Strauss, B. H. (2019). New elevation data triple estimates of global vulnerability to sea-level rise and coastal flooding. *Nature communications*, *10*(1), 1–12.

Lin, N., Emanuel, K., Oppenheimer, M., & Vanmarcke, E. (2012). Physically based assessment of hurricane surge threat under climate change. *Nature Climate Change*, *2*(6), 462–467.

Lin, N., Kopp, R. E., Horton, B. P., & Donnelly, J. P. (2016). Hurricane sandy's flood frequency increasing from year 1800 to 2100. *Proceedings of the National Academy of Sciences*, *113*(43), 12071–12075.

Lin, N., Marsooli, R., & Colle, B. A. (2019). Storm surge return levels induced by mid-to-late-twenty-first-century extratropical cyclones in the northeastern united states. *Climatic change*, *154*, 143–158.

Liu, M., Vecchi, G. A., Smith, J. A., & Knutson, T. R. (2019). Causes of large projected increases in hurricane precipitation rates with global warming. *NPJ climate and atmospheric science*, *2*(1), 38.

Mandli, K. T., & Dawson, C. N. (2014). Adaptive mesh refinement for storm surge. *Ocean Modelling*, *75*, 36–50.

Marsooli, R., Lin, N., Emanuel, K., & Feng, K. (2019). Climate change exacerbates hurricane flood hazards along us atlantic and gulf coasts in spatially varying patterns. *Nature communications*, *10*(1), 1–9.

Miura, Y., Mandli, K. T., & Deodatis, G. (2021). High-speed gis-based simulation of storm surge–induced flooding accounting for sea level rise. *Natural Hazards Review*, *22*(3), 04021018.

Moftakhari, H. R., Salvadori, G., AghaKouchak, A., Sanders, B. F., & Matthew, R. A. (2017). Compounding effects of sea level rise and fluvial flooding. *Proceedings of the National Academy of Sciences*, *114*(37), 9785–9790.

Müller, M. (2011). Rapid change in semi-diurnal tides in the north atlantic since 1980. *Geophysical research letters*, *38*(11).

Neal, J., Schumann, G., & Bates, P. (2012). A subgrid channel model for simulating river hydraulics and floodplain inundation over large and data sparse areas. *Water Resources Research*, *48*(11).

Neumann, B., Vafeidis, A. T., Zimmermann, J., & Nicholls, R. J. (2015). Future coastal population growth and exposure to sea-level rise and coastal flooding-a global assessment. *PloS one*, *10*(3), e0118571.

Reed, A. J., Mann, M. E., Emanuel, K. A., Lin, N., Horton, B. P., Kemp, A. C., & Donnelly, J. P. (2015). Increased threat of tropical cyclones and coastal flooding to new york city during the anthropogenic era. *Proceedings of the National Academy of Sciences*, *112*(41), 12610–12615.

Sarhadi, A., Rousseau-Rizzi, R., Mandli, K., Neal, J., Wiper, M. P., Feldmann, M., & Emanuel, K. (2024). Climate change contributions to increasing compound flooding risk in new york city. *Bulletin of the American Meteorological Society*.

Strauss, B. H., Orton, P. M., Bittermann, K., Buchanan, M. K., Gilford, D. M., Kopp, R. E., … Vinogradov, S. (2021). Economic damages from hurricane sandy attributable to sea level rise caused by anthropogenic climate change. *Nature communications*, *12*(1), 1–9.

Studholme, J., Fedorov, A. V., Gulev, S. K., Emanuel, K., & Hodges, K. (2022). Poleward expansion of tropical cyclone latitudes in warming climates. *Nature Geoscience*, *15*(1), 14–28.

Wahl, T., Jain, S., Bender, J., Meyers, S. D., & Luther, M. E. (2015). Increasing risk of compound flooding from storm surge and rainfall for major us cities. *Nature Climate Change*, *5*(12), 1093–1097.

Westerink, J. J., Luettich, R. A., Feyen, J. C., Atkinson, J. H., Dawson, C., Roberts, H. J., … Pourtaheri, H. (2008). A basin-to channel-scale unstructured grid hurricane storm surge model applied to southern louisiana. *Monthly weather*

review, *136*(3), 833–864.
Wing, O. E., Lehman, W., Bates, P. D., Sampson, C. C., Quinn, N., Smith, A. M., … Kousky, C. (2022). Inequitable patterns of us flood risk in the anthropocene. *Nature Climate Change*, *12*(2), 156–162.
Xi, D., Lin, N., & Smith, J. (2020). Evaluation of a physics-based tropical cyclone rainfall model for risk assessment. *Journal of Hydrometeorology*, *21*(9), 2197–2218.
Zhang, Y., & Najafi, M. R. (2020). Probabilistic numerical modeling of compound flooding caused by tropical storm matthew over a data-scarce coastal environment. *Water Resources Research*, *56*(10), e2020WR028565.

Figure 1. Surge simulation process for ETCs using dynamically downscaled WRF simulations of primary drivers (wind speed and sea level pressure fields) in the study area. (A) Three nested grids with spatial resolutions of 27, 9, and 3-km used for dynamically downscaling WRF simulations (in this study, we focus on the 3-km spatial resolution domain). (B-C) Hourly wind and pressure fields downscaled via WRF simulations driven by ERA-Interim reanalysis for an ETC event occurred on 27-28th December 2012. (D) Simulated surge height (in meters) from the ETC at the regional scale using modified GeoClaw. (E) Performance evaluation of GeoClaw for the ETC storm (the blue line represents observed surge heights during the landfall of the ETCs, calculated by de-tiding water levels, with water elevation subtracted from NOAA tide predictions at the Woods Hole gauge. The red line represents surge heights simulated by GeoClaw. Note that the temporal resolution on the x-axis is six minutes).

Figure 2. Impact of key drivers of compound flooding, such as rainfall intensity and surface wind speed. The top panels include the Probability Distribution Function of rainfall intensity (mm/hr) at each grid cell during landfall and the maximum surface wind speed (knots) at the eye of synthetic TC tracks, both before and at the time of landfall, for two selected synthetic TCs in the current climate downscaled by NCEP reanalysis data. The lower panels depict the corresponding compound flooding response for the two synthetic TCs. (A and B) show the drivers and compound flooding for TC track 1337, while (C and D) show the same results for synthetic TC track 1339.

Figure 3. Comparison of compound flooding risk assessment relative to individual surge and rainfall-driven flooding, and linear addition of individual hazards. (A) Maximum compound flooding level from a randomly selected synthetic TC generated from the EC-EARTH3 model during the late 20th century, along with the location of a coastal area chosen for comparing different types of flooding. (B-C) Flooding levels as a function of the return period from various individual and compound flooding hazard sources for the selected coastal area, using synthetic TCs generated from the CESM2 model for the late 20th and 21st centuries, respectively. (D-M) Similar to (B-C) but using synthetic TCs generated from other climate models. The shaded areas in the plots represent sampling uncertainty bounds, calculated based on the 5th and 95th percentiles of a Poisson distribution within each climate model.

Figure 4. Assessment of the contribution of SLR and changes in TC climatology to the risk of compound flooding in the late 20th and 21st centuries, focusing on the selected location depicted in Figure 3 (A). Each line in the graph illustrates the simulated compound flooding levels derived from synthetic TCs downscaled from each of the six climate models. The shaded region represents the confidence interval, indicating sampling uncertainty, and is calculated based on the 5th and 95th percentiles of a Poisson distribution within each climate model.

Figure 5. Impact of TC climatology change and SLR on the alteration of compound flooding risk during today's climate (2000-2020) in comparison to the late 20th century (1979-1999) in a selected coastal location. (A) representation of the compound flooding levels as a function of return period, comparing today's climate with the late 20th century. The results are derived from the depicted coastal location, excluding intertidal zones. Each line represents compound flooding outcomes produced through the generation of synthetic TCs based on reanalysis NCEP data for the respective time periods. The shaded areas in the figure indicate the sampling uncertainty margins, calculated using the 5th and 95th percentiles of a Poisson distribution. (B) Assessment of the impact of changes in TC climatology and SLR on the spatially-varying risk of 100-year return period compound flooding events in today's climate relative to the late 20th century. In this map, red color denotes an increasing trend, blue color represents a decreasing trend, and gray color signifies areas exhibiting no discernible trend or values close to zero.

Figure 6. Impact of TC climatology changes and SLR on compound flooding in historical, present, and future climates in the selected coastal area (depicted in the left panels). Each line represents the outcomes derived from synthetic TCs downscaled from multiple climate models and reanalysis data for the three timeframes: historical (dark blue), present (light blue), and future climates (red). The shading in the figure represents confidence intervals (5% and 95%) derived through a bootstrapping approach for the ensemble of climate models. See text for details.

Figure 7. Spatially distributed granular risk of compound flooding from TCs in past and future climates. (A-D) Present the results of compound flooding for various return periods in the late 20th century. (E-H) Depict the same analysis for the late 21st century. (I-L) Illustrate the differences in compound flooding levels between the late 21st century and late 20th century for different return periods. Here, red indicates an increasing trend, blue indicates a decreasing trend, and gray signifies no clear trend or values close to zero. Note that these results are based on the ensemble mean of the six CMIP6 climate models.

Figure 8. Impact of ETC climatology changes and SLR on the risk of compound flooding in the current and future climates in the selected coastal area (depicted in the left panels). Each line represents the outcomes derived from dynamically downscaled ETC events for two timeframes: the current climate (2006-2020, shown in blue) and future climates (2081-2100, shown in red). The shading in the figure represents confidence intervals (5% and 95%) derived through a bootstrapping approach.

Figure 9. Spatially distributed granular risk of compound flooding from ETCs in the current and future climates. (A-D) Present the results of compound flooding for various return periods in the current climate. (E-H) Depict the same analysis for the late 21st century. (I-L) Illustrate the differences in compound flooding levels between the late 21st century and the current climate for various return periods. Note that red indicates an increasing trend, blue indicates a decreasing trend, and gray signifies no clear trend or values close to zero.